TRACE ELEMENT FINGERPRINTING IN THE GULF OF MEXICO VOLCANIC ASH

by

CHRISTINA JONES

B.S,. UNIVERSITY OF RHODE ISLAND, 2005

A THESIS

Submitted in partial fulfillment of the requirements for the degree

MASTER OF SCIENCE

Department of Geology
College of Arts and Sciences

KANSAS STATE UNIVERSITY
Manhattan, Kansas

2008

Approved by:

Major Professor
Dr. Matt Totten

Abstract

Sands rich in volcanic ash have been encountered within the late Cenozoic sequence offshore Louisiana in the northern Gulf of Mexico. These beds are identified on well logs by their high radioactivity and low density. Paleontologic markers used to date these deposits give dates that are consistent with eruptions from the Snake River Plain (SRP) and Yellowstone calderas. Lead isotope ratios from the Gulf of Mexico samples are also consistent with the SRP-Yellowstone tuffs. The objective of this study was to compare the rare earth element (REE) and other trace element data from the GOM samples to determine whether they may be differentiated from one another, and also whether they compare to the SRP data.

Well cuttings and sidewall core samples from sixteen wells known to contain volcanic ash were density separated using lithium metatungstate to isolate the low-density volcanic glass from the remaining minerals. The concentrated ash was dissolved and analyzed using ICP-MS. Trace and REE variations were plotted by depositional age based upon paleontological markers.

Variations in most trace elements are not useful criteria for discriminating ash by age. There is a wide spread in fairly mobile elements (i.e. Sr, Ba), suggesting that each ash bed has had a different diagenetic history. REE variations, in particular the magnitude of the Europium anomaly and the degree of fractionation between light and heavy REE, are good discriminates of each ash. A few anomalous samples plot within an older field, which might be explained by reworking of older ash into younger deposits. Direct correlation to SRP-Yellowstone eruptions is hindered by the lack of SRP samples analyzed using similar methods.

Table of Contents

List of Figures

List of Tables

Acknowledgements

I would like to acknowledge first my major professor Matt Totten for help and guidance through this project and time at Kansas State. Both my committee members Iris Totten and Sam Chaudhuri who helped me improve my project and teach me many useful things. I am also grateful for research and financial support from GCAGS, and KGS. Thank you to Shell, Exxon and Chevron for the use of samples.

Chapter 1 Introduction

Ash in the Gulf of Mexico

In literature as early as the 1920's volcanic sediments were observed for the Gulf Coast and the Gulf of Mexico (GOM). It wasn't until the 1970's that more extensive research of volcanic ash in the Gulf of Mexico began. Literature for volcanic ash and the GOM include Kennett and Huddleston, (1972) with the first documented attempt of combining tephrachronology and biostratigraphy. Other work includes Hunter and Davis, (1979) with maps of volcanic sediment distributions from the Cretaceous to present (Rather, 1999). Beginning in the late 1970's, exploratory drilling activity in the deepwater Gulf of Mexico (GOM) focused on Pliocene and Pleistocene sandstone reservoirs. Many of the target locations were determined by accompanying technological advances in direct hydrocarbon indicators (DHI) using seismic reflection data. DHI depends upon the density contrast between sandstones containing significant low-density hydrocarbons and the surrounding sedimentary beds. This has been a very successful exploration strategy in the GOM, and continues to be used extensively today. On occasion, however, some of the target sandstones do not contain hydrocarbons, but instead contain a significant proportion of volcanic glass shards. These shards are also of low density, and will cause a comparable density contrast as the hydrocarbon bearing sandstones.

Volcanic ash-containing sandstones have been identified in many locations across the Gulf of Mexico (Figure 1.1and 1.2). These are distributed widely across the Gulf, from sandstones of variable age (Hanan et al., 1998). The thicknesses of the deposits are variable, with some ash-rich beds over 300 feet thick. The thickness of the deposits and their association with other sediments suggests they are not all volcanogenic air-fall. It is believed the deposits have been reworked from previously ash falls.

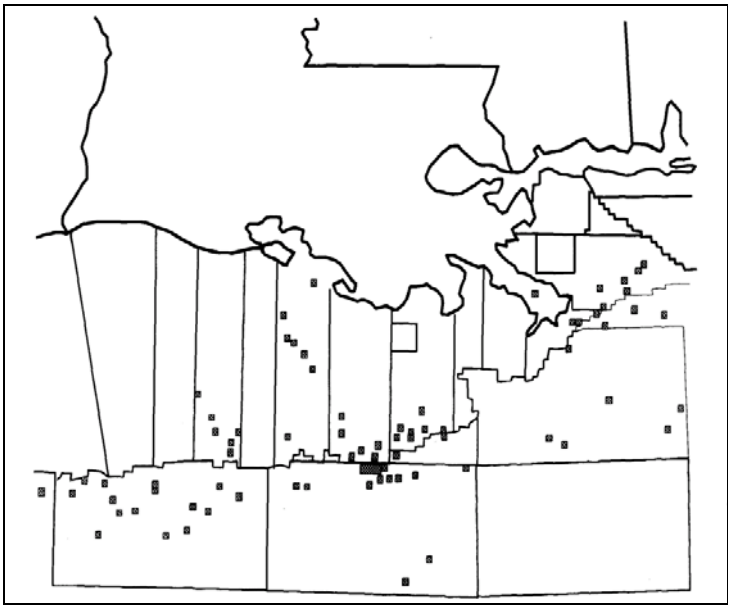

Figure 1.1 Potential location of wells with ash based on well log attributes (Hanan et al., 1998).

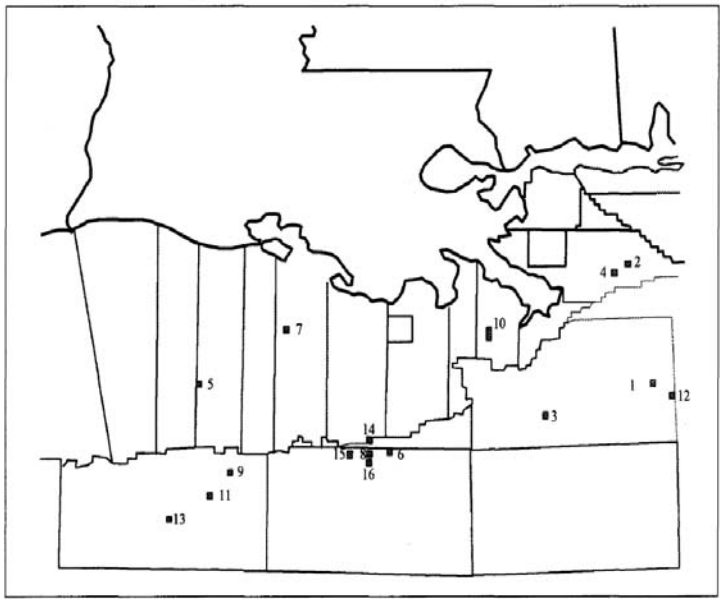

Figure 1.2 Confirmed locations of wells with ash in the GOM using (Hanan et al., 1998).

Potential Sources of Ash

The source of the GOM ash-rich deposits is still a subject of debate. Many previous workers have suggested that it was from Central America or Mexico (Ledbetter, 1985). Their evidence has largely been based upon the relatively short transport distance, and that dispersal of modern eruptions into the GOM has been witnessed. Other workers have presumed that the ash was from west Texas, which is commonly recognized as the source for ash-rich material within Oligocene sandstones such as the Frio or Catahoula formations (Walton, 1986).

Volcanic activity in west Texas ceased at the end of the Oligocene (Walton, 1986). There are no volcanic centers in this region coincident with the Miocene to Pleistocene aged ash-rich sandstones within this study. An identical argument is also valid for most of the Mexican sources. Volcanic activity in this region also declined significantly before the end of the Miocene (Moreno, 1994).

Central American sources are still actively contributing ash to the GOM. Two lines of evidence rule these sources out as contributors to the ash-rich deposits in this study. The first is a lack of a mechanism to concentrate the ash into the extremely thick deposits (up to 300' thick) reported in Totten et al. (2005). The Central American ashes are distributed in millimeter thick deposits in the deepest part of the GOM basin. The ashes from the Plio-Pleistocene trend in this study are within quartz-rich sandstones, and occur on the deep shelf or upper slope. How would these thin deposits be so extensively thickened and moved upslope? How would they be mixed with material so obviously from the continent?

Just as convincingly, the chemical compositions of the Central American ashes are not the same. The Central American eruptions are much more mafic in composition than the GOM ash. An average Central American ash is comprised of approximately 50% silica, while the GOM ash shards average approximately 75% silica (Van Fleet et al., 1999).

These two lines of evidence suggest the source of these ash-rich beds is not local. An obvious potential source was the western US. A list of major eruptions from the western United States with the eruption age is given in Table 1.1. These ages were compared to the approximate age of the GOM ash, which was determined using

paleomarkers. Paleontological markers (usually defined by one or more index fossils) are used by the petroleum industry to identify the stratigraphic position during drilling. This data is available from the Minerals Management Service of the Department of the Interior. The makers nearest the GOM ash beds were identified, and used to date the ash beds (Kratochvil, 1997).

Tuff Name	Location	Age	Reference
Lava Creek	Yellowstone Plateau, WY	0.61	Christiansen,1984
Bishop	Long Valley, CA	0.74	Bailey, et al., 1976
Upper Bandelier	Jemez Mts., NM	1.12	Self, et al., 1986
Mesa Falls	Yellowstone Plateau, WY	1.27	Christiansen,1984
Lower Bandelier	Jemez Mts., NM	1.45	Self, et al., 1986
Huckleberry	Yellowstone Plateau, WY	2.0	Christiansen,1984
Nomlaki	Cascade Range, CA	3.4	Sarna-Wojcicki,et al., 1991 (Denag)
Kilgore	Heise, Snake River, WA	4.3	Morgan, et al., 1984; Morgan, 1988
Walcott	Heise, Snake River, WA	6.0	Morgan, et al., 1984; Morgan, 1988
Black Tail Creek	Heise, Snake River, WA	6.5	Morgan et al., 1984; Morgan, 1988
City of Rocks	Picabo or Heise, Snake River Plain, ID	6.5	Leeman, 1982
McMullen Creek	Twin Falls, Snake River Plain, ID	8.6	Williams, et al., 1990
Wooden Shoe Butte	Twin Falls, Snake River Plain, ID	10.1	Williams, et al., 1990
Ann Arbor	Picabo, Snake River Plain, ID	10.3	Kellogg, et al., 1989
Sublett Range	Twin Falls, Snake River Plain, ID	10.4	Williams, et al., 1982
Wilson Creek	Twin Falls, Snake River Plain, ID	11.0	Ekren, et al., 1984
Grasmere	Bruneau-Jarbridge, ID	11.2	Bonnichsen, 1982
Cougar Point III	Bruneau-Jarbridge, ID	11.3	Bonnichsen, 1982
Browns Creek	Twin Falls, Snake River Plain, ID	11.4	Ekren, et al., 1984
Steer Basin	Twin Falls, Snake River Plain, ID	12.0	Williams, et al., 1990
Badlands	Humboldt, Snake River Plain, ID	12.0	Ekren, et al., 1984

Table 1.1 List of the major Western U.S. eruptions from the Pleistocene, Pliocene and Miocene modified from (Hanan et al. 1998).

Figure 1.3 shows the close agreement between these two datasets. There are definitely ample western US eruptions to source the GOM deposits. Comparison of the fetch area of several eruptions (Izett and Wilcox, 1982) to the Mississippi drainage basin shows that it is possible to deliver ash from the continent to the GOM (Figure 1.4).

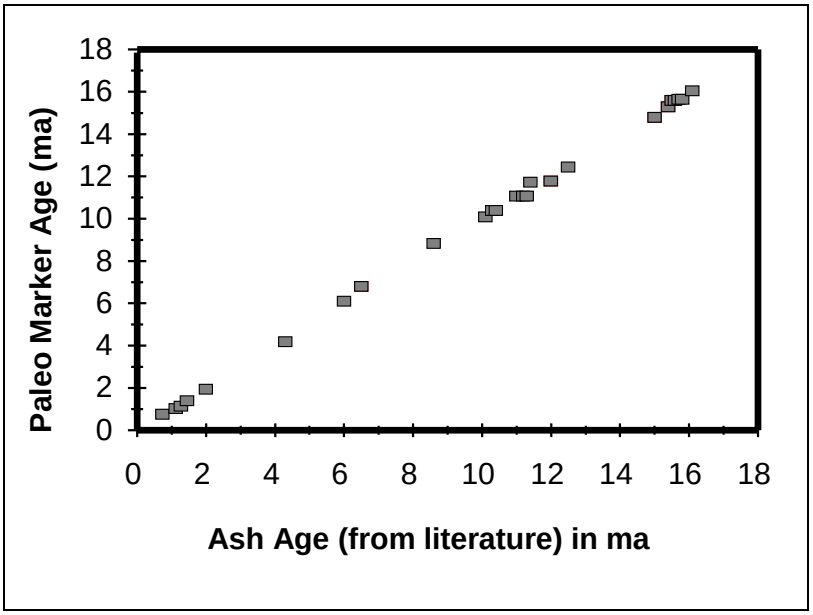

Figure 1.3 A comparison of paleo marker and ash ages from literature in million of years, modified from (Totten et al., 2005).

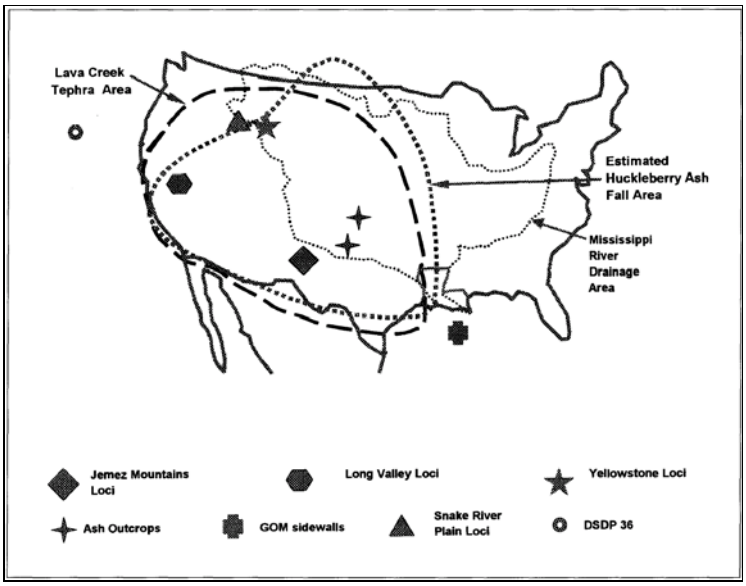

Figure 1.4 Map of the U.S. outlining the fetch areas of the Lava Creek and Huckleberry Ridge ash falls. The loci of major eruption centers and ash outcrops are indicated by different symbols (Hanan et al. 1998).

Preliminary trace-element and isotopic signatures from a previous work support the SRP /Yellowstone eruptions as sources for the GOM ash. Hanan et al. (1998) showed the similarity between lead isotopes from the GOM and Yellowstone volcanism as reported in the literature (Figure 1.5). Individual eruptions from Yellowstone were differentiated. Kachler (1999) reported that Pliocene ash from the GOM could be differentiated from Pleistocene shards using trace elements. Her data was hindered by the high detection limits provided by DCP analyses. It did suggest that trace element signatures held promise, as more sensitive indicators were used.

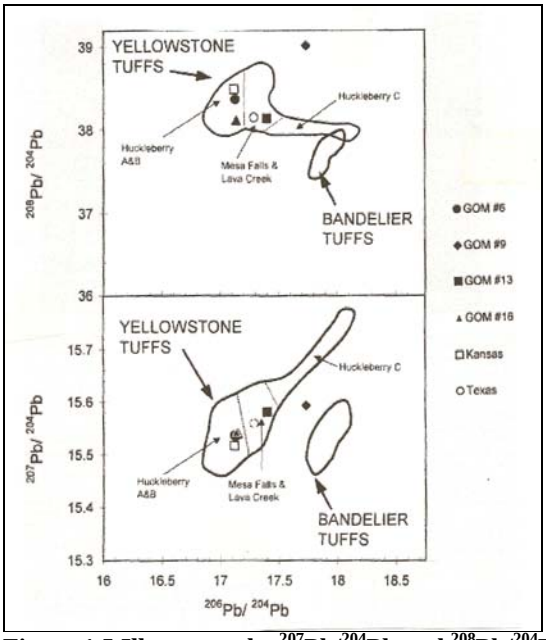

Figure 1.5 Illustrates the $^{207}Pb/^{204}Pb$ and $^{208}Pb/^{204}Pb$ verses $^{206}Pb/^{204}Pb$ co-variation diagrams with GOM, Kansas and Texas samples. Six samples fall within the Huckleberry Ridge A, B, C (3 different eruptions) Mesa Falls, or Lava Creek (Hanan et al. 1998).

Objectives

The objective of this study was to investigate these ash-rich sandstones in the Gulf of Mexico to determine if they could be differentiated using rare earth element and other trace element geochemistry. The SRP has been proposed as the likely source of the

ash in the GOM (Totten et al., 2005, Hanan et al., 1998). The age of the GOM ash as determined by paleontology correlates with the timing of SRP eruptive events (Kratochvil, 1997). Preliminary geochemical analyses of the GOM ash show them to be compatible with the chemical signature of SRP volcanic rocks (Hanan et al., 1998). The focus of the study was to widen the previous studies in scope, and to fingerprint each occurrence to a specific eruption in the SRP area.

Establishing eruptive sources for each specific ash found in the GOM will lead to better control on the stratigraphic and well correlation in the Gulf of Mexico. Comparisons of the eruption age to depositional age based upon paleontological markers will better constrain the timing of sediment dispersal from the continent to deepwater. Ultimately, the benefit of this study might lead to better understanding of the eruptions themselves, from offshore deposits because of their more complete preservation than on the continent.

Chapter 2 Background

Western United States Volcanic Activity

In the western United States there are many different volcanic provinces including the Southwestern Nevada, the Thomas Range and the Snake River Plain volcanic fields. The early Cenozoic from 45 to 17 Ma was marked by widespread calc-alkaline volcanism. Around 18-14 Ma major basaltic centers included the Columbia River Basalt (CRB), Steens Basalt Mountain (SB) and Northern Nevada rift (NNR). Bimodal basalt and rhyolite volcanism became widespread from 17 to 15 Ma marking a change from calc-alkaline volcanism (Perkins and Nash, 2002). Around 17 to 16 Ma a relatively short inactive period took place after which the late Cenozoic volcanism began (Luedke and Smith, 1991). The volcanic activity in the late Cenozoic was dominated by a bimodal system. The system started with silicic magma composition, and then changed to mafic magma composition (Perkins et al., 1998).

The silicic volcanic activity began 16.6 Ma along the Yellowstone hotspot track on the Nevada-Oregon border. At the same time basaltic centers like the Columbia River Basalt and centers in the south were reaching their peak with rhyolitic centers starting in

the south (Perkins and Nash, 2002). Throughout the rest of the Western U.S. there were smaller more isolated areas of basaltic volcanism (Luedke and Smith, 1991). During the period from 5 to 10 Ma the volcanic activity was not as extensive or covered as much area as the activity mentioned above. Despite this fact there was activity in northeast California, southern Oregon, northern Nevada, southwest Idaho, and the southwest and south Colorado Plateau

Beginning five million years to present the volcanic centers in many places became fixed and began to show linear patterns of calderas (Luedke and Smith, 1991). The Snake River Plain is an example of a linear progression to the northeast through time. The Snake River Plain consists of an elongated southern path with two provinces in west central Idaho. To the east the Snake River Plain extends to the northwest and merges with the Yellowstone Plateau in northwest Wyoming (Luedke and Smith, 1991).

Geochemical investigations of the Snake River Plain and Yellowstone volcanic system have been conducted by a number of scientists. One such study includes work by Bindeman and Valley (2001) that looked at $\delta^{18}O$ values from individual phenocrysts from rhyolites in the Yellowstone plateau. The study of Bindeman and Valley (2001) focuses on pre and post caldera collapse tuffs to examine the relationship between normal and low $\delta^{18}O$ rhyolites (Bindeman and Valley, 2001).

Trace elements play an important role in volcanic systems. They are naturally a focus of investigation of the GOM ashes. Some of the major and trace element data from the Bindeman and Valley (2001) study is presented below. Sr/Rb and Ba/Rb ratios were used to look at any chemical differences between low $\delta^{18}O$ and normal $\delta^{18}O$ rhyolites. The early members of Huckleberry Ridge and Lava Creek tuffs are characterized by lower Sr and Ba, higher Rb and a resulting low Sr/Rb. Trace element results for Ba/Rb and Zr/Rb verse Sr/Rb can be found in Figure 2.1.

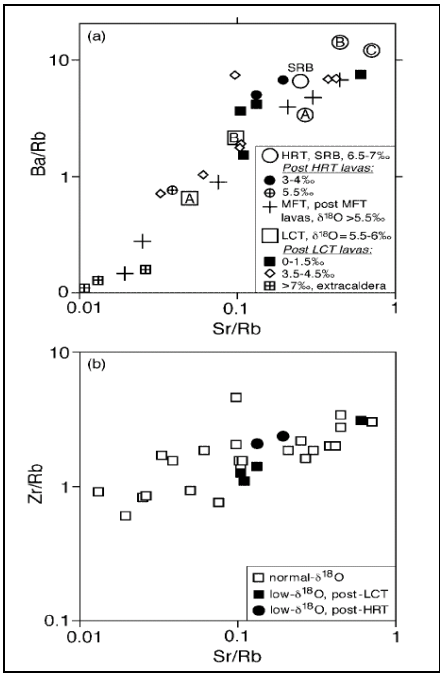

Figure 2.1 Results for Ba/Rb and Zr/Rb vs. Sr/Rb from whole rock lave and tuff samples. Fractional crystallization values from feldspar for Sr and Ba and Zr from zircons (Bindeman and Valley, 2001).

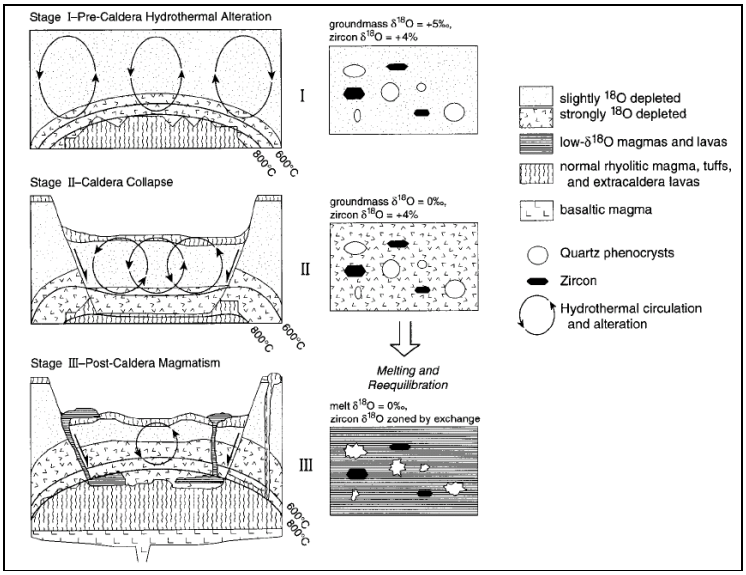

Figure 2.2 Diagrams illustrating the hypothesized method for delta ^{18}O value depletion in post caldera lavas in Yellowstone (Bindeman and Valley, 2001).

Snake River Plain and Yellowstone Plateau

The two areas active in the Northern Province were the High lava Plains in Oregon and the Snake River Plains in Idaho. The Snake River Plain and Yellowstone volcanic field is a sequence of calderas tending NE to SW covering 800 km. The Yellowstone hotspot track is marked by silicic centers getting younger to the northeast and marks the north perimeter of the Basin and Range Province (Perkins et al., 1998). In the south there are two loci of volcanic activity, one small and large in the western Snake River Plain (west-central Idaho). The larger loci is an old structural basin filled with thick sedimentary deposits topped with basalt tholeiitic flows and Pliocene and early Pleistocene shield volcanoes. The smaller loci is a canyon filled with basaltic lavas form the Boise River and South Fork tributary erupted from cinder cones 2 million years old and younger (Luedke and Smith, 1991). The silicic centers of the hotspot are grouped into two categories the "Orevado" province on the west, older in age (16.5 to 14.5 Ma) and the Snake River Plain volcanic province on the east younger in age (<15 Ma). In the Snake River Plain volcanic province the silicic rocks are mainly metaluminous rhyolite lavas and ash tuffs. The "Orevada" province contains ash tuffs of peralkaline rhyolite with some metaluminous rhyolites. This proves there is a sight difference in the ash tuffs from the older 16.6 to 14.5 Ma eruptions and the younger < 15 Ma eruptions within the SRP. The "Orevada" province includes the calderas, High Rock, McDermitt (M), and Lake Owyhee or Owyhee Humboldt (OH) 15.2 Ma. The Bruneau-Jarbudge (BJ) 12.7 Ma, Twin Falls (TF) 10.5 Ma, Picabo (P) 10 Ma, and Heise (H) 6.6 Ma calderas fall in line next (Perkins et al., 1998).

During the Pliocene into the Pleistocene the Yellowstone Plateau (YP) 2.1 Ma contains three calderas the Huckleberry Ridge (HR) 2.06 Ma, Mesa Falls (MF) 1.30 Ma and the Lava Creek (LC) 0.60 Ma (Perkins and Nash, 2002). This string of calderas is called the Yellowstone hotspot track (Figure 2.3).

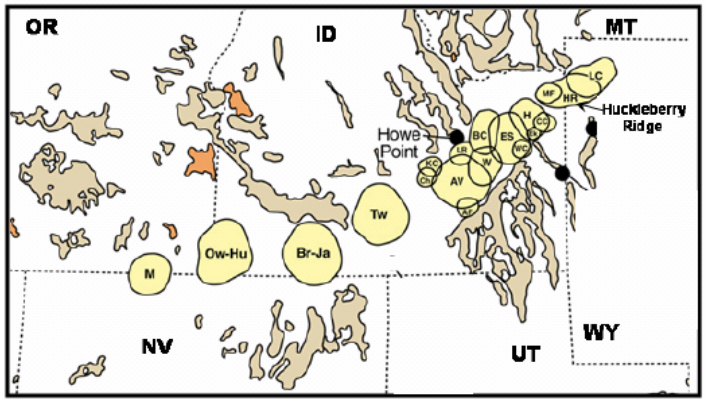

Figure 2.3 Map of the Yellowstone hotspot track with caldera centers represented by circles with abbreviations (HR) Huckleberry Ridge, (MF) Mesa falls, and (LC) Lava Creek, modified from (Totten et al., 2005).

The hotspot track is marked by explosive silicic volcanic centers (Perkins and Nash, 2002). The silicic rocks along the Yellowstone hotspot track in general are rich in Fe, poor in Ca, and low in phenocrysts dominated by quartz (Perkins and Nash, 2002). In terms of the ash fall record for the hotspot there are three stages of volcanic activity. The three magmatic stages are based on ages, M1 (metaluminous stage 1) 16-15.2 Ma, M2 15.2-7.5 Ma and M3 7.5-0 Ma (Perkins and Nash, 2002). Each stage has a distinctive magma composition, and frequency of eruptions. The M1 stage is characterized by increased concentrations of incompatible elements like Rb and a decrease in Mn/Fe. Stage M2 has increased concentrations of compatible elements, but a decrease in incompatible elements. Stage M3 has higher Cl, Mn/Fe concentrations and lower Rb concentrations. The frequency difference for the three stages shows a trend of decreased eruption frequencies from M1 to M3 (Perkins and Nash, 2002). By the time these ashes make it to the GOM the Mn, Fe, compatible, and incompatible compositions have averaged out so the ratios listed above are not as useful for the GOM ash as for ash in the area.

The Huckleberry Ridge tuff produced an estimated 8.2 million km^3 of silicic rich ash. The waste area the Huckleberry Ridge ash includes much of the Mississippi River drainage basin (Figure 1.4). Izett and Wilcox (1982) described ash deposits as far west as California, east as Kansas, and South as Texas. Some deposits including one in Nevada was described as Fluvial (Izett and Wilcox, 1982) and Meade County Kansas as reworked

(Naser et al. 1973). Once these ash air fall deposits were incorporated into the Mississippi River drainage basin tributaries would transport the reworked ash to the Gulf of Mexico. In the Gulf of Mexico onshore of Louisiana Yellowstone ashes have been described which is over 1,200 miles from the Yellowstone calderas (Hanna, 1926). The ash rich sediments carried form the Mississippi River system gets deposited as turbidities ash-rich in the Gulf of Mexico deep water (Hanan et al 1998).

Supervolcanos

The shear size of some of the late Cenozoic eruptions has only recently been recognized (Christiansen, 1984). The magnitude of these eruptions has resulted in a new paradigm, the supervolcano (Bindeman, 2006). Supervolcanic eruptions were initially overlooked, partially because they have not been witnessed in recorded history, but also because the scale of the associated calderas was not easily observed without the perspective gained from orbital flight. The subsequent recognition of the Snake River Plain (SRP) and the adjoining Yellowstone Plateau as a series of huge, supervolcanic calderas created as the North American continent drifted across the Yellowstone hotspot followed (Bindeman, 2006). The Yellowstone Plateau volcanic system is one of the biggest centers for silicic volcanism in the world (Bindeman and Valley, 2001). The system is characterized by large volume ignimbrite eruptions with caldera collapse following. The tuffs occurred as followed the Huckleberry Ridge (~ 2 Ma) with ~ 2,500 km^3 , Mesa Falls (~1.3 Ma) with ~300 km^3 , and Lava Creek (~0.6 Ma) with 1,000 km^3 (Bindeman and Valley, 2001). In between the tuff eruptions were $\delta^{18}O$ depleted rhyolite lava and domes erupted and the volume of the post Lava Creek tuff was ~900 km^3. Figure 2.4 shows the Yellowstone Plateau and the vicinity with the location of the calderas and lava flows.

The cycle proposed by Bindeman (2006) includes four steps. One the partial melting of mantle material above the subducting plate which pools in the lower crust while the lower mantle chamber is a replenishing pool. Two involves a bulging of the chamber in the lower crust so a build up of pressure causes fractures and vents. Three is the violent eruption producing a pyroclastic flow spreading out tens of kilometers in all directions. Four is the formation of a caldera over the mostly drained magma chamber,

with some lava flows but no violent eruptions. The cycle will then start over after the system recharges (Bindeman, 2006). This recognition of the shear volume of eruptions has led to the identification of ash deposits of previously unknown provenance across a wide portion of the continent as being sourced from SRP eruptions (Izett and Wilcox, 1982).

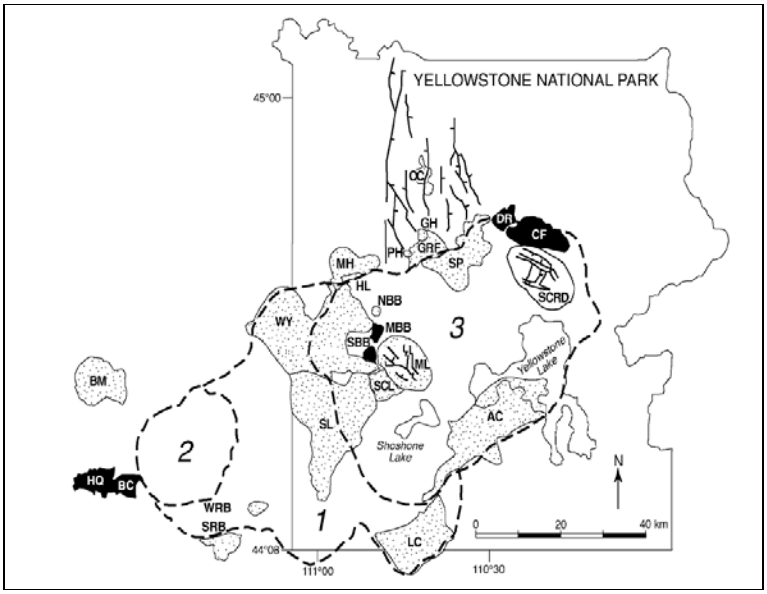

Figure 2.4 Map of the Yellowstone National Park lava flows and calderas. Calderas in dashed lines 1) Big Bend 2) Henry Fork 3) Yellowstone. Black indicates low 18O flows and all other flows and domes are in a black dot pattern (Bindeman and Valley, 2001).

Geology of the Gulf of Mexico

The north central Gulf of Mexico (GOM) is the one of the most extensively researched basins and Figure 2.5 is a map of this region. This area is of great interest because of the petroleum deposits common in the region. This region contains the block areas where the volcanic ash samples were found. The basin has a diameter around 1500 Km or 931 miles and contains Triassic to Holocene sedimentary rocks with thickness up to 10-15 Km or 6-9 miles (McBride et al., 1998). There are three sub provinces, the deep water (>1500 ft), subsalt (100 to a couple 1,000 ft), and suprasalt (0-1500 ft), all of which overlap (Weimer et al., 1998).

Figure 2.5 Gulf of Mexico leasing map showing the north central Gulf Coast off of Louisiana from (Mineral Management Services).

The Gulf of Mexico formed as a result of rifting and the crust stretching when the North American plate moved apart from the South American and African plates during the late Triassic and early Jurassic. During the early Jurassic along with stretching and rifting a thick deposit of the Callovian salt occurred (Weimer et al., 1998). The Callovian salt was later remobilized and played a part in migration and trapping petroleum in the region. The crust had thinned from around 69 to 76% and subsidence during the Mesozoic was greatest in the central basin caused from thermal effects (McBride et al., 1998). As a result the deep GOM was covered by1 Km of water and interpreted as having a water shale and marl sequence (Weimer et al., 1998). Sedimentation post rifting (middle Jurassic to early Cretaceous) consisted of shallow marine platform carbonates

along the edges of the northern GOM with thick continental crust underneath (Weimer et al., 1998). During this time there was periodic inflow of siliciclastic sediments. During the Cenozoic subsidence was greatest at the northern border caused by sedimentary loading. During this time continental siliciclastic sediments drainage was caused by the Laramide orogeny in the U.S. and Mexico (Weimer et al., 1998). It wasn't until the Miocene that all sediments from the central U.S. started to drain into the northern GOM around Louisiana. The Ewing Bank and Green Canyon area is dominated by allochthonous salt and extension features including growth faults, salt welds and folds. The bathymetry is a mixture of turbidity deposits in the form of minibasins between allochthonous salt deposits. The turbidity deposits serve as reservoirs for the northern GOM. Sediment loading caused salt to deform from the original autochthonous layers with a variety of allochthonous salt geometries (Weimer et al., 1998).

The ash samples are from wells located in blocks from the northern GOM including Grand Isle and Green Canyon. This area is located on the present upper slope and outer shelf offshore Louisiana. The water depths for the region range from 200 ft in the north and 4500 ft in the south. The modern bathymetry is irregular because of complex salt tectonics with intraslope basins from the Pliocene and Pleistocene (Weimer et al., 1998). The sediments from the Pliocene and Pleistocene include turbidity deposits in minibasins which can be up to 20,000 ft thick. There were several different environments for sediment deposition including channels, lobes, over banks, and slides (Weimer et al., 1998).

Rare-Earth Elements (REE)

Rare earth elements (REE) contain the elements on the periodic table from La to Lu (atomic numbers 57-71). Another name for the REE is the lanthanide series. When looking at how the REE behave both the ion radius and charge are important. Ionic radius shows a decreasing trend from La to Lu. The REE are commonly divided into two groups: the light (La-Sm) and the heavy (Eu-Lu). The decrease in ionic radii towards Lu results in the heavy REE being preferentially incorporated into the crystallizing mineral phases, while the light REE remain in the magma melt. This is the reason why light REE are more enriched than the heavy REE in evolved magmas. The common oxidation state

of the REE is $^{+}3$, with the exception of Ce^{+4} and Eu^{+2}. If plagioclase is crystallizing, Eu^{+2} can substitute for Ca^{+2}, causing a negative Eu anomaly in the melt. The anomaly is calculated by dividing the actual Eu value by the expected value assuming a constant slope of the REE at Eu. If the Eu value falls above the REE slope the anomaly is greater than one (positive), if it falls below the REE slope than the value is less than one (negative).

Chapter 3 - Methods

In the Northern Gulf of Mexico there have been many wells with confirmed ash bearing intervals and many which have yet to be studied. The Gulf of Mexico is divided into regions known as protraction areas. Within each area there are variable numbers of different blocks, and each block is 3 square miles. Some of the common locations for ash are in the Green Canyon, Ewing Bank, Ship Shoal and South Timbalier areas.

In the GOM, the number and type of analytical procedures is constrained by the small quantities of material recovered and preserved during drilling operations. The 16 GOM ash samples used in this study were collected from both well cutting from previously recognized ashes and other confirmed ash bearing units identified by well log characteristics. For ash to register from a well log there has to be a minimum of 5% ash content in the sandstone, but some samples contain up to 30 % ash. The well cuttings were density-separated to concentrate the ash shards using the method of Totten et al. (2005). This method uses a variable density liquid to separate solid phases by density. The weight percentage of this material was recorded and noted to contain primarily ash. The 16 concentrated ash samples were analyzed for trace and rare earth element compositions using ICP-MS from the University of Kansas Plasma Analytical Laboratory (KU-PAL) during the fall 2007. Once the data for both minor and trace elements was obtained comparisons to the literature and any possible patterns to finger-print the ashes could be examined.

Ash Identification by Well Logs

Well logs were used to identify potential intervals of interest. The main indicators used are the relationship between the Gamma Ray (GR) and Spontaneous Potential (SP) log curves. Other indicators include bulk density and sonic logs. The natural gamma radiation in sediments is measured by GR tool. Ash beds and shale contain higher GR readings than sandstones. In shale's the high GR reading is caused by potassium, but with volcanic ash thorium produces the high GR. In some cases spectral GR logs can measure individual radiometric components like potassium, uranium and thorium. The SP curve can help distinguish if the high GR is from shale or another lithology like ash. In ash beds the GR and Sp curves are inverted and can cross each other. One ash example the Huckleberry Ridge with a grain density of 2.3 g/cc results in a bulk density log showing a difference between the ash and the more dense sediments around it (Hanan et al., 1998). Sonic logs are used to measure the velocity of acoustic waves through a certain substance. In the case of rocks the velocity is slower than with the low density ash layers. Figure 3.1 shows a GR and SP curve with the ash interval highlighted.

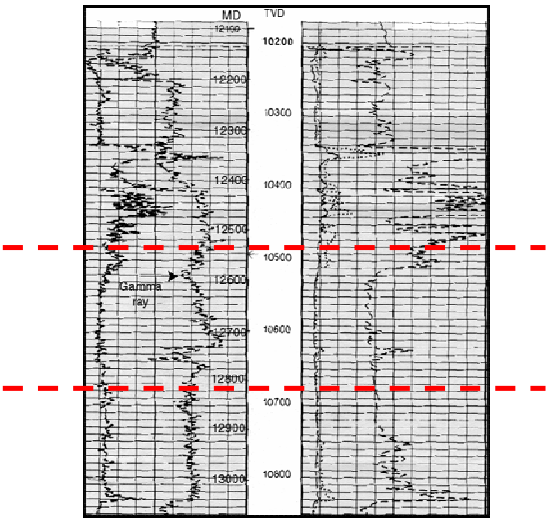

Figure 3.1 Well log for GC 16 showing the ash interval enclosed but the red dash line, modified from a presentation by (modified from Rather, 1999).

Paleontology Reports

After the potential ash samples were identified the first step was to obtain the paleontology reports. The paleontology reports allow for an approximate age range for

the ash samples. Microfossils serve as markers for particular age ranges. Several paleontological markers are used to bracket the interval of interest for the sample wells (Jurik, 2003). A common industry marker used is Lenticulina 1 or foraminifera Marginulinopsis lacrimata (2.2 to 2.3 MA). Another common marker (DTR 10) used is the last appearance datum (LAD) for the nannofossil Discoaster brouweri at 1.8 MA (Berggren et al., 1995). Other nannofossils used are Discoaster pentaradiatus (2.2 MA), and foraminifera Globorotalia miocenica (2.2 MA). Discoaster pentaradiatus (2.2 MA) in many cases is the most common marker expected below the Huckleberry Ridge ash (Rather, 1999). The Globorotalia miocenica (2.2 MA) is associated with depths over 300 feet (90 meters) and the Lenticulina 1 (2.2 to 2.3 MA) from shallow deeps 0 to 300 feet (Rather, 1999). Many of the paleomarkers mentioned above are available to the public by the Mineral Management service. Figure 3.2 gives an example of a biostratigraphic chart used for paleo bracketing in the GOM.

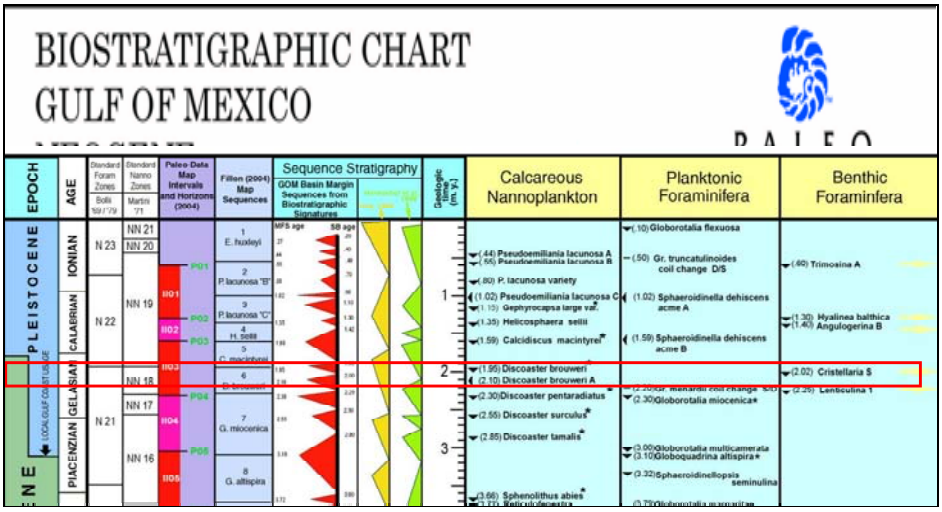

Figure 3.2 Example of a biostratigraphic chart used for paleo bracketing. Red box outlines the time that would include the Huckleberry Ridge eruption from presentation by (Totten et al., 2007).

Sample Preparation and Separation

In the case of well sample types sidewall cores are preferred over drill cuttings. The reason drill cuttings are harder to work with is sampling depth uncertainty. A

mudlogger is used to collect cuttings directly at the well but have a 30 ft interval of uncertainty (Jurik, 2003). The opposite is true with sidewall cores which are obtained by a wireline tool and the exact depths are known. The samples used in this study contain but sidewall cores and drill cuttings. Each well sample had ~2 grams separated weighted and disaggregated if necessary with a mortar and pestle. The samples were then soaked in distilled water and disaggregated again in an ultrasonic bath. The cleaned samples were run through a 10-micron micro-sieve using a Fisher Scientific 550 Sonic Dismembrator. The sample can then be poured into a cup and dried in an oven (Jurik, 2003 and Rather 1999). Figure 3.3 show an Image of ultrasonic cleaning and micromesh sieves.

Figure 3.3 Image of the Ultrasonic cleaning and micromesh sieves.

The density separation of the ash samples used the method from Totten et al. (2002) developed for use in separating clay mineral samples. Lithium metatungstate (LMT) which is an water based inorganic, non-toxic salt was used because it is safer to handle, easier to adjust the specific density, and gives a greater range of specific densities (Hanan and Totten, 1996). A test tube filled with LMT can be seen in Figure 3.4. Traditional liquids used are halogenated hydrocarbons examples tetra-bromoethane and bromoform (Totten et al, 2005). Other common liquids used are ammonium metatungstate and sodium metatungstate (Hanan et al, 1996).

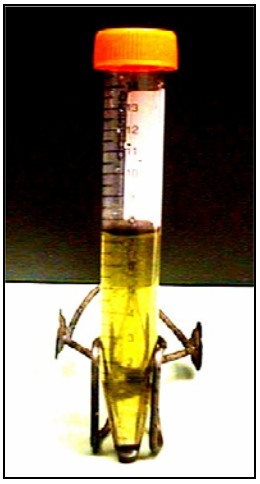

Figure 3.4 Image of lithium metatungstate used in the density separation of ash.

Lithium metatungstate is the heaviest metatungstate available and can be purchased from Commercial Testing & Engineering Co. Denver Co (Hanan and Totten, 1996). With clay minerals the traditional liquids tend to absorb to the surface of the minerals. Also certain clay minerals like smectite will absorb the organic heavy liquids preferentially over other minerals making the density separation less effective (Totten et al, 2002). Beyond these complications there is the problem with handling, using, recycling and disposal. With lithium metatungstate plastic or stainless steel containers and distilled water should be used because insoluble Ca–metatungstate can precipitate with free Ca^{+2} ions (Hanan and Totten, 1996). With the LMT solution the specific gravity (G) can be adjusted with distilled water ranging from 1.0 to 3.4. The LMT can be reuse, by recovering through evaporation at low temperature (< 100°C). If LMT crystallizes into a solid it is hard to re-dissolve. Although this method was developed from use in clay and heavy mineral separations it lends itself well for ash separation (Totten et al, 2002).

The LMT solution is kept at room temperature 25ºC and to obtain different stock solutions with specific gravity of 3.1 was diluted by adding distilled water. To figure out the amount of distilled water to add the formula $V_w = (V_o\rho_f - V_o\rho_o)/ (\rho_w - \rho_f)$ was used. In the equation above V_w = volume of distilled water, V_o = volume of stock solution, ρ_f = final density required, ρ_o = density of the stock solution, and ρ_w = density of water at lab temperature (Totten et al, 2002). By weighting the LMT needed to fill a 25mL

pycnometer the density of the working solution was found the solutions were then stored in air tight containers. Around 1g of the dried sediment samples were placed into 50 mL polycarbonate centrifuge tubes with screw on lids. To suspend the mixture the tubes were shook then centrifuged for one hour at 3000 rpm keeping the temperature constant (Totten et al, 2002). To help with dense material trapped in the lighter fraction the float portion was re-suspended then centrifuged for another hour. The test tube was then frozen with a N_2 liquid bath and the thin layer at the top was removed by washing with a distilled water and acetate filtering apparatus (Totten et al, 2002). This layer is recovered and contains most of the material least than the specific gravity of the LMT solution. The material in the sink layer is the material with a specific gravity greater than the LMT solution. There may be some material near the specific gravity of the LMT solution in the float layer that didn't have time to sink (Totten et al, 2002). The reason of the LMT solution was melted and any liquid above the sink layer removed slowly with a micro-pipette and saved. This step minimizes the LMT still in tube to dilute the solution for the next suspension (Totten et al, 2002). Even if the liquid appears to be clear of any material Stoke law calculations suggest the liquid will still contain some super fine grains. The next suspension is conducted in the same manner with the material at a smaller specific gravity (Totten et al, 2002). An SEM and microscope image of ash from Green Canyon 16 (GC 16) can be seen in Figure 3.5.

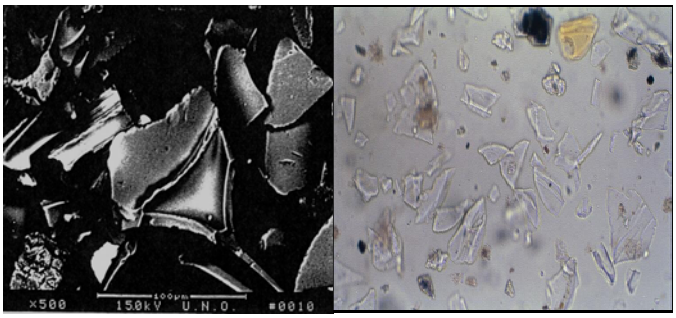

Figure 3.5 An SEM image of the left and microscope image (depth 12,560 ft MD) on the right from Green Canyon 16 (GC 16) ash from presentation by (Totten et al., 2007).

ICPMS

The University of Kansas Plasma Analytical Laboratory (KU-PAL) contains a Fisons/VG PlasmaQuad II+XS Inductively Coupled Plasma Mass Spectrometer (ICPMS). The ICPMS extracts positively-charged ions from plasma using a 27 MHz RF generator. The ICP-MS is equipped with a three-channel peristaltic pump (sample introduction, spray chamber drain, and autosampler-probe continuous wash). Also a Gilson 222XL autosampler with full X-Y-Z capabilities is included. The RSD error is less than 1% with precision and sensitivity in measuring isotope abundances. A dual detector system (Channeltron electron multiplier) allows signals of high sensitivity (pulse-counting de) and lower sensitivity (analog mode) to be collected. Seamless data can be collected with wide concentration range because of cross calibration between the detectors.
(http://www.geo.ku.edu/programs/researchFacilities/PALwebPage0311/PALpageFacMS.htm

Figure 3.6 Image of the Fisons/VG PlasmaQuad II + XS Inductively Coupled Plasma Mass Spectometer (ICPMS) from the University of Kansas (KU-PAL) website.
http://www.geo.ku.edu/programs/researchFacilities/PALwebPage0311/PALpageFacMS.htm

Chapter 4 – Results

The outcome of the density separations resulted in sixteen samples that were utilized in this study. Figure 4.1 is a map of location of the samples. The well locations, depths, and paleontological markers are given in Table 4.1. The bulk of the samples are equivalent in age to the Huckleberry Ridge eruption, with two samples equivalent to the

Mesa Falls, and four that have an age of approximately 7 million years in the late Miocene.

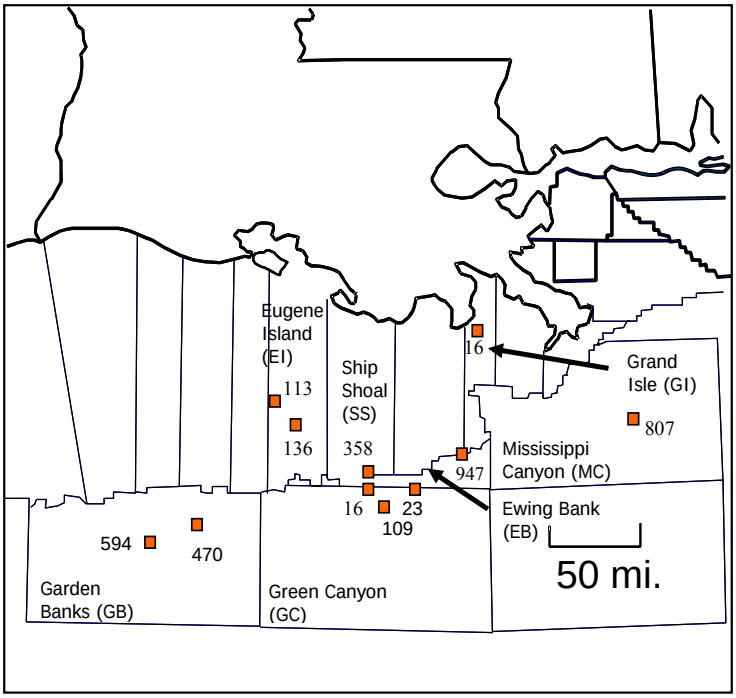

Figure 4.1 Map of well locations for ash samples used in this study (modified from Hanan et al., 1998).

Log images of Individual ash samples

The seismic well logs played an important role in the identification of ash bearing units within the GOM. An example of a well log from GC 16 can be found in Figure 4.2. Well log images for other GOM ash samples are presented below with the interval of interest with high gamma ray readings outlined.

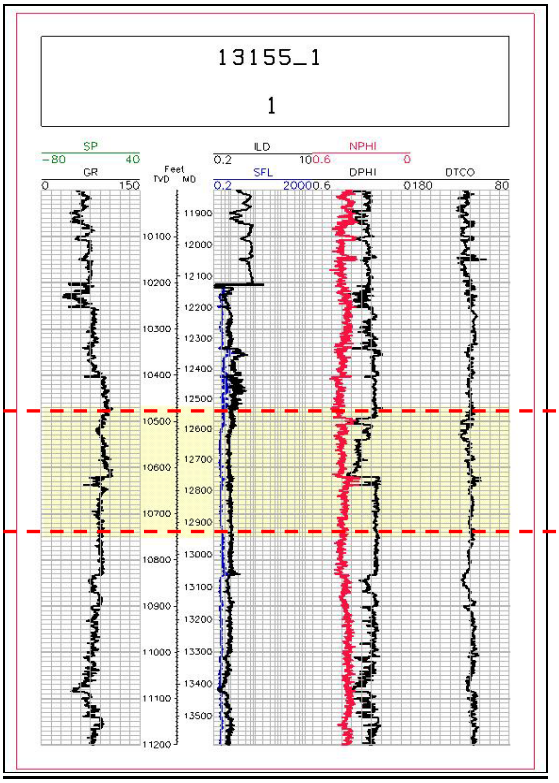

Figure 4.2 Well log for GC 16, red dashed lines note the interval ash was observed and black dashed lines the highest weight % of ash modified from (Jurik, 2003).

Above the well log for GC 16 is presented indicating the highest weight % of ash found within the interval from 12,530' to 12,950' MD and up to 10% ash weight (Rather, M.A., 1999).

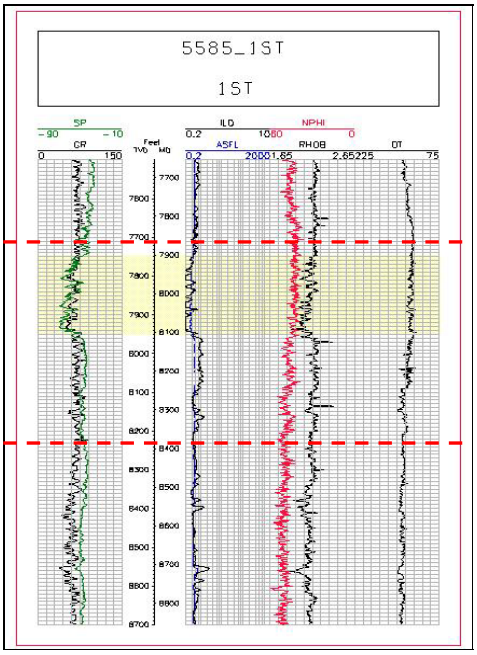

Figure 4.3 Well log for sample from SS 358 from a side track well. Red dashed lines outline the interval with ash modified from (Jurik, 2003).

Deleted: inveral

The well logs in figure 4.3 correspond to sample OCS 5585 #1 ST from the block SS 358. Ash was found within the interval form 8,449' to 8,461' with ash weight from 13 to 30 to 35%.

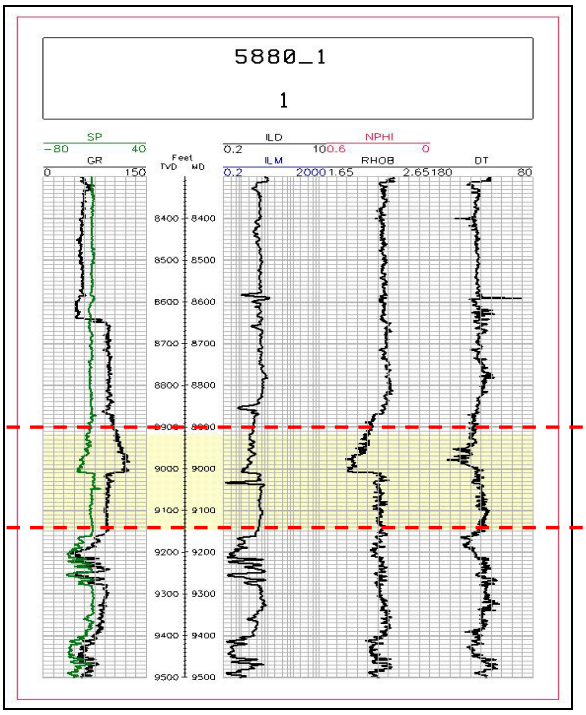

Figure 4.4 Well log for GC 23, red dashed lines outline the ash interval modified from (Jurik, 2003).

The well log corresponds to both OCS 5880 #1 cuttings and sidewall both from GC 23. Samples were found in the interval from 8,917' to 9,147' MD (Hanan et al., 1998).

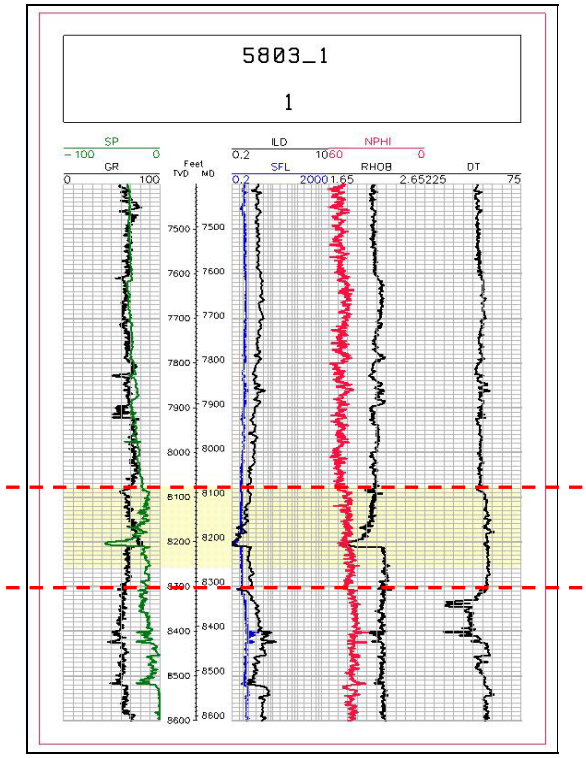

Figure 4.5 Well log for EB 947, red dashed lines outline ash interval modified from (Jurik, 2003).

The well log above corresponds to OCS 5803 #1 from EB 947. Around 200 ft of ash found in the interval from 8,110' to 8,300' contained 5 to 29% ash weight.

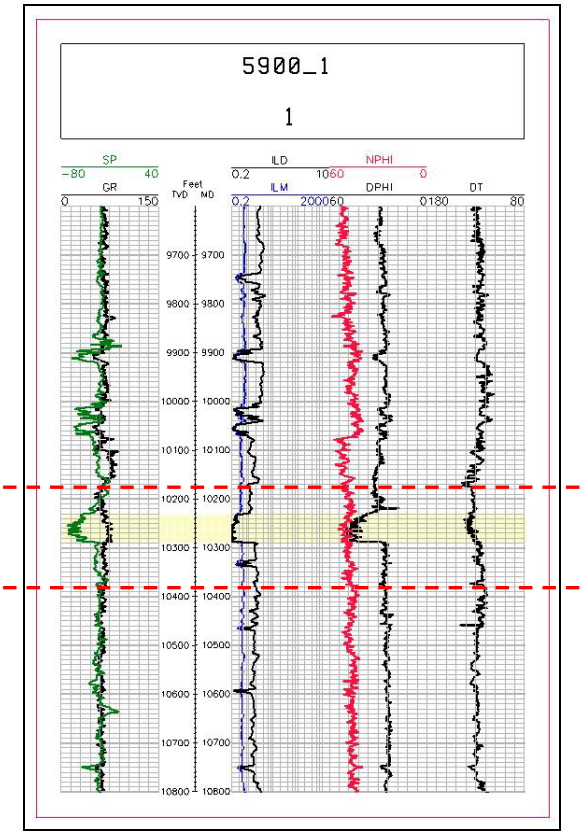

Figure 4.6 Well log for GC 109 A-1, red dashed lines outline the ash interval modified from (Jurik, 2003).

The well log above corresponds to 5900 A-1 from GC 109 A-1. The ash interval is around 60 ft from 10,230' to 10,290' MD.

Rare Earth and Minor Element Data

The results for both the rare-earth (La through Lu) and minor element values for the 16 Gulf of Mexico ash samples are found below. The University of Kansas Plasma Analytical Laboratory (KU-PAL) Fisons Inductively Coupled Plasma Mass Spectrometer (ICPMS) was used to obtain all geochemical data. Table 4.1 lists all 16 samples with block numbers, offshore coastal shelf (OCS) number and eruption age.

Sample #	OCS #	Block #	Paleo Marker	Paleo Age (Ma)	Estimated Eruption Age
1	12650' Unocal 13155 #1	GC 16a	D. brouweri	1.95-2.0	HR
2	12680' Unocal 13155 #1	GC 16b	D. brouweri	1.95-2.0	HR
3	12680' Unocal 13155 #1	GC 16c	D. brouweri	1.95-2.0	HR
4	12770' Unocal 13155 #1	GC 16d	D. brouweri	1.95-2.0	HR
5	5900 #A-1	GC 109 A-1	NP1.78	1.95-2.0	HR
6	5900 #A-2	GC 109 A-2	NP1.78	1.95-2.0	HR
7	5880 #1 cuttings	GC 23a	NP1.78	1.95-2.0	HR
8	5880 #1 sidewall	GC 23b	NP1.78	1.95-2.0	HR
9	5585 #1ST	SS 358	D. brouweri	1.95-2.0	HR
10	5803 #1	EB947	NP1.78	1.95-2.0	HR
11	11548 #1	GB 594	P1.58-P1.6	1.04-1.15	Mesa Falls/Band.
12	8248 #A-20	GB 470	P1.58	1.07	Mesa Falls
13	031 #P38	GI 16	*Cristellaria K.	~7	Miocene
14	7963 #A-14	MC 807	M 2.2	7.75	Miocene
15	4442 #1	EI 113	*Cristellaria K.	~7	Miocene
16	3152 #JA-1	EI 136	M 2.2	7.75	Miocene

Table 4.1 List of all 16 GOM ash samples with paleo marker, age, eruption age based on the paleo data, block #, OCS # and sample #. (GI 16 paleo pick from (Steiner, 1973).

The raw rare earth data and chondrite normalized values from (Taylor and Mclennan, 1995) for the GOM ashes can be found respectively in Tables 4.2 and 4.3. Both tables include the estimated age based on the paleontological assemblage picks, presumed eruption, block and OCS number. Tables 4.2 through 4.6 identify the 16 samples by sample number. In Table 4.3 the expected (Eu*) value was calculated using formula 1 below. The Eu anomaly is the difference between the actual Eu and Eu* value using formula 2. Both the Eu* and Eu anomaly were calculated using the following formulae.

$(Sm + Gd)/2 = Eu^*$

$Eu/Eu^* = Eu$ anomaly

The chondrite normalizing values used from (Taylor and Mclennan, 1995) can be found in table 4.4. In Tables 4.2, 4.3, 4.5, and 4.6 the (*) next to the paleo marker indicate the company the data was gathered from.

(*) = Exxon

(**) = Shell

Sample #	La	Ce	Pr	Nd	Sm	Eu	Gd	Tb	Dy	Ho	Er	Tm	Yb	Lu
1	70.3	134	14.1	58.2	11.6	0.61	10.09	1.87	10.8	2.10	6.37	0.99	6.30	0.90
2	55.5	107	11.2	46.6	9.27	0.74	8.24	1.41	7.83	1.51	4.66	0.70	4.39	0.65
3	72.3	138	14.4	59.6	12.1	0.63	10.7	1.96	11.1	2.18	6.88	0.99	6.44	0.94
4	66.3	127	13.2	54.4	11.0	0.65	9.74	1.73	9.9	1.94	6.09	0.88	5.71	0.83
5	58.8	111	11.6	48.4	9.63	0.12	13.6	1.44	8.15	1.58	5.04	0.74	4.71	0.68
6	59.0	111	11.5	47.7	9.73	not detected	13.6	1.46	8.40	1.64	5.23	0.77	4.94	0.72
7	59.4	112	11.6	47.9	9.69	0.60	8.43	1.52	8.75	1.73	5.53	0.82	5.19	0.76
8	82.1	153	15.5	64.5	13.3	0.86	12.0	2.21	12.9	2.49	7.71	1.22	7.43	1.10
9	45.2	85.2	9.55	37.0	7.21	0.60	11.5	1.05	5.72	1.14	3.31	0.52	3.35	0.52
10	78.7	150	16.5	62.9	12.5	0.73	12.0	2.04	11.7	2.34	6.68	1.04	6.54	0.98
11	70.9	131	12.5	50.3	10.8	0.69	9.9	1.97	11.7	2.19	6.72	1.30	7.10	1.05
12	23.9	45.1	4.89	18.8	3.77	0.42	3.77	0.54	2.87	0.59	1.73	0.28	1.84	0.28
13	47.9	95.3	8.51	36.1	7.52	0.86	8.73	1.04	4.60	0.94	2.70	0.42	2.61	0.39
14	35.7	67.7	7.44	32.7	6.66	0.97	9.18	0.82	4.49	0.79	2.23	0.41	2.40	0.35
15	58.3	113	12.4	47.0	8.91	1.14	8.27	1.32	7.19	1.44	4.18	0.67	4.33	0.67
16	27.5	54.7	5.95	26.3	5.26	0.89	5.60	0.64	3.49	0.65	2.05	0.37	3.21	0.36

Table 4.2 List of the raw earth values obtained using the ICPMS from the University of Kansas Plasma Analytical Laboratory (KU-PAL).

Sample #	La	Ce	Pr	Nd	Sm	Eu	Gd	Tb	Dy	Ho	Er	Tm	Yb	Lu	Eu*	Eu/Eu*
1	191.6	140	103.2	81.9	50.2	7.00	32.97	32.16	28.3	24.68	22.81	27.71	25.42	23.67	41.58	0.168
2	151.2	112	81.8	65.5	40.15	8.53	26.93	24.30	20.55	17.76	16.70	19.60	17.72	17.13	33.54	0.254
3	197.1	144	105.4	83.8	52.2	7.28	35.0	33.76	29.2	25.62	24.68	27.70	25.95	24.57	43.62	0.167
4	180.8	132	96.4	76.5	47.6	7.47	31.82	29.79	26.1	22.78	21.83	24.77	23.01	21.73	39.69	0.188
5	160.2	116	84.7	68.1	41.68	1.38	44.5	24.74	21.39	18.53	18.07	20.80	19.00	17.95	43.08	0.032
6	160.6	116	83.8	67.1	42.12	1	44.4	25.18	22.05	19.27	18.74	21.57	19.90	19.02	43.27	0.023
7	161.8	117	84.7	67.4	41.93	6.90	27.56	26.28	22.96	20.28	19.81	22.98	20.95	20.03	34.74	0.199
8	223.6	160	113.5	90.7	57.6	9.89	39.2	38.02	33.9	29.26	27.62	34.38	29.94	28.81	48.37	0.204
9	123.1	89.0	69.69	52.0	31.23	6.90	37.6	18.13	15.02	13.40	11.86	14.69	13.52	13.62	34.4	0.201
10	214.3	157	120.1	88.5	54.3	8.37	39.3	35.18	30.7	27.53	23.96	29.26	26.36	25.75	46.79	0.179
11	193.1	137	91.2	70.7	47.0	7.91	32.5	33.97	30.7	25.76	24.09	36.43	28.62	27.51	39.73	0.199
12	65.2	47.1	35.67	26.5	16.31	4.79	12.33	9.28	7.53	6.89	6.21	7.92	7.42	7.34	14.32	0.334
13	130.6	99.5	62.09	50.8	32.54	9.94	28.52	17.87	12.08	11.00	9.67	11.80	10.52	10.15	30.53	0.325
14	97.3	70.8	54.28	45.9	28.82	11.17	30.00	14.15	11.78	9.23	8.01	11.56	9.68	9.13	29.41	0.380
15	159.0	119	90.5	66.0	38.56	13.10	27.04	22.77	18.86	16.88	14.98	18.73	17.45	17.51	32.8	0.399
16	74.9	57.1	43.43	37.1	22.77	10.21	18.31	11.02	9.17	7.59	7.34	10.43	12.93	9.39	20.54	0.497

Table 4.3 Chondrite normalized values for the rare earths using (Taylor and Mclennan, 1995). Includes the Eu* and Eu anomaly values. Eu value in red was estimated because Eu not detected in sample 6.

La	**0.3670**
Ce	**0.9570**
Pr	**0.1370**
Nd	**0.7110**
Sm	**0.2310**
Eu	**0.0870**
Gd	**0.3060**
Tb	**0.0580**
Dy	**0.3810**
Ho	**0.0851**
Er	**0.2790**
Tm	**0.0356**
Yb	**0.2480**
Lu	**0.0381**

Table 4.4 Values used to normalize the rare earths to chondrite (Taylor and Mclennan, 1995).

The raw minor element values for the 16 GOM ashes can be found in table 4.5 and the ratios of these elements in table 4.6.

Sample #	Ba	Rb	Th	Sr	Nb	Pb	U	Y	Zr
1	1811	103	25.7	65.4	44.6	40.0	6.57	69.1	192
2	2926	98.1	21.3	80.7	33.0	32.0	5.07	47.3	179
3	2751	104	26.4	89.4	47.1	41.8	6.78	69.7	199
4	1997	101	24.7	78.4	44.6	109	6.25	61.8	191
5	20037	118	18.4	409	36.5	35.6	4.36	52.2	160
6	23465	126	18.9	391	38.2	33.8	4.54	54.4	159
7	1544	147	20.0	108	30.1	32.9	4.90	56.3	162
8	421	179	27.1	5.96	2.96	34.0	6.67	80.3	234
9	17396	104	13.5	368	25.4	121	3.62	37.9	159
10	594	170	26.7	40.9	48.9	40.6	6.63	76.4	246
11	757	245	31.9	195	32.1	37.6	7.59	74.2	192
12	5553	83.6	8.18	156	11.6	16.5	2.42	19.8	77.4
13	13883	59.9	12.7	195	17.5	32.5	3.16	30.8	359
14	15197	110	10.26	330	2.49	36.4	3.34	25.4	93.3
15	4071	142	22.2	112	34.6	43.7	6.06	46.9	351
16	2341	26.4	8.17	308	0.68	15.9	2.33	21.1	109

Table 4.5 List of the minor elements found in the GOM ashes.

Sample #	Ba/Rb	U/Th	La/Lu	La/Sm	Sr/Rb	Zr/Rb
1	17.61	0.26	8.09	3.82	0.636	1.86812
2	29.82	0.24	8.82	3.77	0.823	1.8258
3	26.42	0.26	8.02	3.78	0.859	1.90827
4	19.70	0.25	8.32	3.80	0.773	1.88856
5	169.60	0.24	8.93	3.84	3.459	1.35707
6	186.33	0.24	8.45	3.81	3.105	1.26365
7	10.52	0.25	8.08	3.86	0.738	1.1036
8	2.35	0.25	7.76	3.88	0.033	1.30912
9	168.02	0.27	9.04	3.94	3.557	1.53643
10	3.50	0.25	8.33	3.95	0.24	1.44871
11	3.09	0.24	7.02	4.11	0.796	0.7852
12	66.44	0.30	8.89	4.00	1.864	0.92559
13	231.88	0.25	12.86	4.01	3.254	5.99186
14	138.48	0.33	10.66	3.38	3.008	0.84983
15	28.64	0.27	9.08	4.12	0.791	2.46912
16	88.81	0.29	7.97	3.29	11.69	4.13126

Table 4.6 REE and other trace element ratios for all GOM ashes.

Sample #	Sample Name	Eruption Age	La	SM	Eu	Gd	Tb	Lu	Eu*	Eu A	La/Sm	Sm/Gd	La
1	HR Kansas	HR	272.48	67.10	9.89	42.81	NA	29.40	54.96	0.18	4.06	1.57	
2	Mesa Falls Tuff	MF	250.68	51.95	10.80	32.68	NA	20.47	42.31	0.26	4.83	1.59	
3	Blacktail Tuff	Miocene	196.19	43.29	14.94	34.61	17.24	21.00	25.92	0.58	4.53	1.25	
4	HR fused obsidian	HR	256.13	69.26	7.01	42.48	NA	28.87	55.87	0.13	3.70	1.63	

Table 4.7 List of other examples of HR, MF, and Miocene ashes with REE data. Data collected from HR Kansas (Totten, personal communication), Mesa Falls Tuff and HR fused obsidian (Christiansen, 2001), and Blacktail Tuff (Morgan et al., 1984).

Sample #	Sr	Rb	Ba	Th	Ce	Zr	Sm	Y	Yb
1	0.5	51	91	128.7	13	2	3.5	2.3	1.85
2	0.7	49	146	106.6	11	2	2.8	1.6	1.29
3	0.7	52	138	131.8	14	2	3.7	2.3	1.89
4	0.7	51	100	123.3	13	2	3.3	2.1	1.68
5	3.4	59	1002	92.2	11	2	2.9	1.7	1.39
6	3.3	63	1173	94.6	11	2	2.9	1.8	1.45
7	0.9	73	77	99.8	11	2	2.9	1.9	1.53
8	0.0	89	21	135.3	15	3	4.0	2.7	2.18
9	3.1	52	870	67.4	9	2	2.2	1.3	0.99
10	0.3	85	30	133.6	15	3	3.8	2.5	1.92
11	1.6	122	38	159.7	13	2	3.3	2.5	2.09
12	1.3	42	278	40.9	5	1	1.1	0.7	0.54
13	1.6	30	694	63.6	10	4	2.3	1.0	0.77
14	2.8	55	760	51.3	7	1	2.0	0.8	0.71
15	0.9	71	204	111.2	11	4	2.7	1.6	1.27
16	2.6	13	117	40.8	5	1	1.6	0.7	0.94

Table 4.8 Trace and REE normalized to MORB using (Pearce, 1983).

Sr	**120.0**
Rb	**2.0**
Ba	**20.0**
Th	**0.2**
Ce	**10.0**
Zr	**90.0**
Sm	**3.3**
Y	**30.0**
Yb	**3.4**

Table 4.9 Values from (Pearce, 1983) used to normalize to MORB.

Chapter 5 Discussion

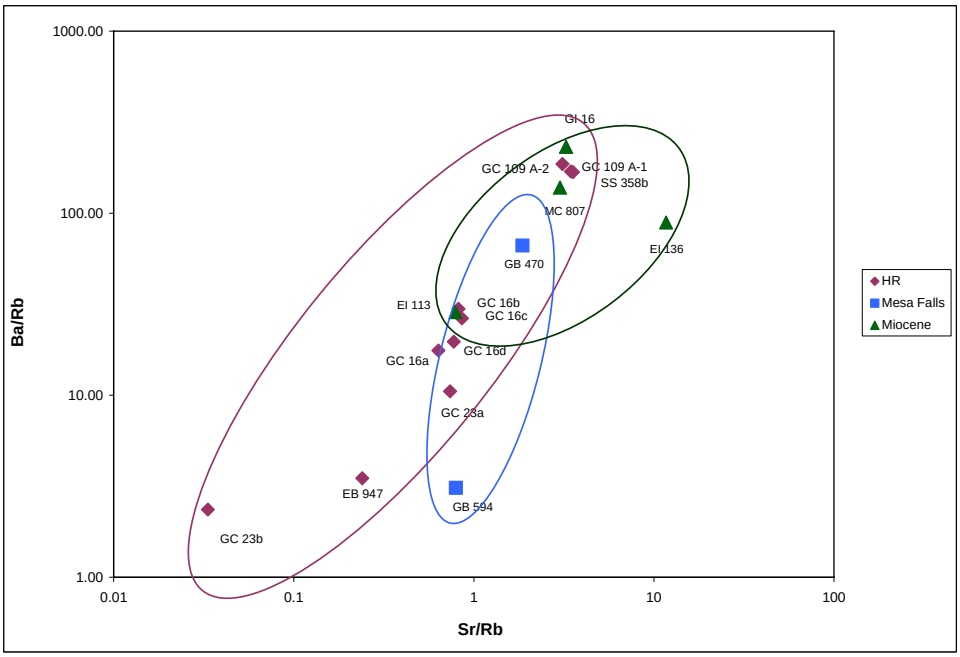

Figure 5.1 Sr/Rb verses Ba/Rb for the GOM ashes.

Figure 5.1 displays the data for the GOM ash samples in a format similar to Figure 2.1 from Bindeman and Valley (2001). The Huckleberry Ridge age ashes have a similar range to the Bindeman and Valley (2001) samples (Ba/Rb 0-10 and Sr/Rb 0.01-1). There are some exceptions with higher Ba/Rb and Sr/Rb values. The Mesa Falls samples follow the same pattern with ranges (Ba/Rb 1-10 and Sr/Rb 0.1-1), with the exception of GB 470. The Huckleberry Ridge, Mesa Falls, and Miocene age equivalent ashes from the GOM fall within the same values as samples from Yellowstone. It is not possible, however, to differentiate between the individual units using these trace elements.

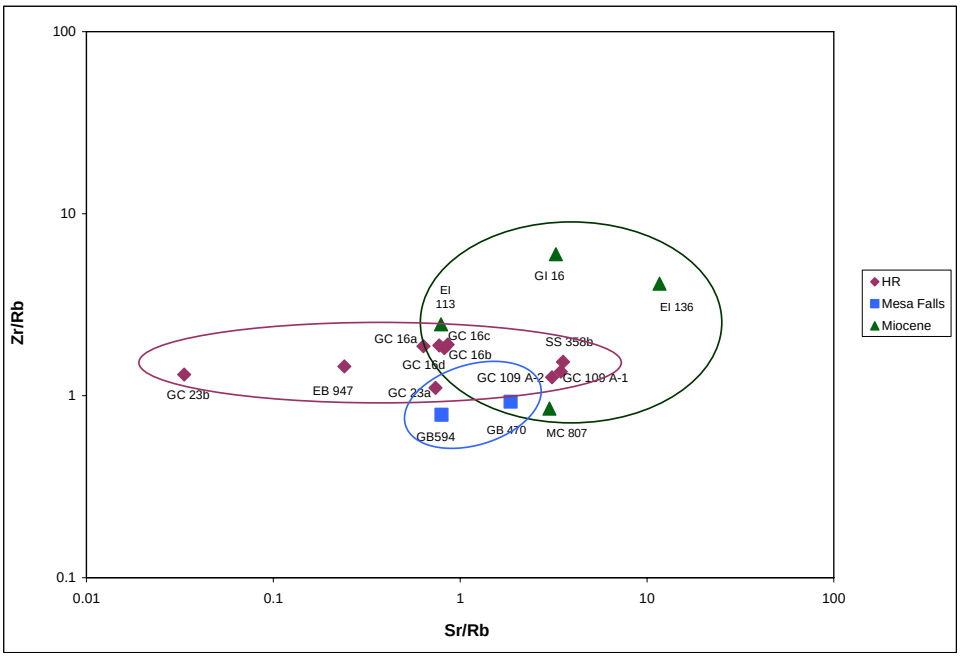

Figure 5.2 Sr/Rb verses Zr/Rb for the GOM ashes.

The plot above displays Sr/Rb versus Zr/Rb for the GOM ash samples like seen in Figure 2.1 from Bindeman and Valley (2001). The Huckleberry Ridge age ashes have a similar range (Zr/Rb 1-10 and Sr/Rb 0.1-1). In general, the Miocene aged samples have higher Sr/Rb than the Huckleberry Ridge-aged samples, but the differences are not significant enough to specifically discriminate between the Huckleberry Ridge, Mesa Falls, and Miocene age ashes.

Rare-earth Element Diagrams

The figures below show the REE diagrams for the Huckleberry Ridge, Mesa Falls and Miocene age GOM ashes. All REE values are normalized to chondrite values (Taylor and Mclennan, 1995). Included is an individual plot for the four GC-16 samples collected at three different depths, to examine any differences (Figure 5.3).

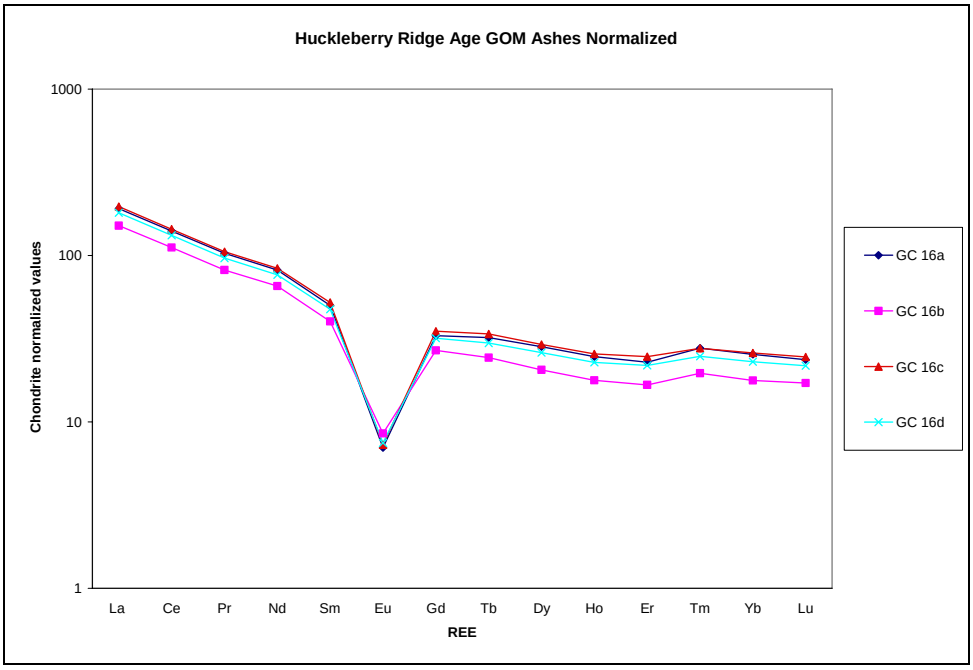

Figure 5.3 REE plot for the GC 16 ash samples.

The four samples for GC 16 were collected at three different depths. GC 16a, GC 16c and GC 16d were collected from drill-cuttings at 12,650ft., 12,680 ft., and 12,770 ft., respectively. GC 16b was collected from a sidewall core at 12,680 ft. All of the samples from drill-cuttings are remarkably similar, implying that there is very little difference with depth within a single ash occurrence. There is a minor difference in the pattern for the sidewall core (GC 16b) compared to the others, with GC 16b illustrating a slightly less fractionation and lower overall REE values. Samples obtained as drill-cuttings are an average over thirty feet of drilling, compared to a sidewall core which is sampled at a precise depth. The difference between GC 16b and GC 16c would, therefore, be a reasonable approximation of the variation within each single occurrence. Samples obtained from drill-cuttings are a natural average of each occurrence with respect to the REE.

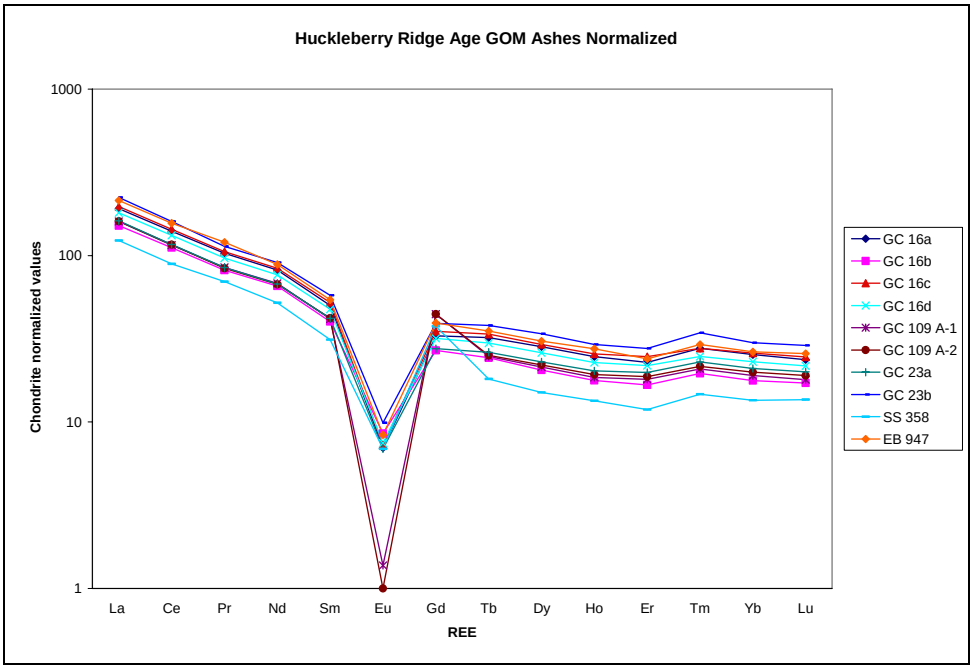

Figure 5.4 REE plot for the Huckleberry Ridge age GOM ashes.

As shown in Figure 5.4, most of the HR-aged ashes have similar REE patterns. Two major differences are samples GC 109 A-1 and A-2 which have the most negative Eu anomaly values of any samples in the study. Other than the Eu anomaly, these samples are consistent with the other HR-aged ash. The only sample that differs is SS 358, which follows the same REE pattern but has lower REE concentrations.

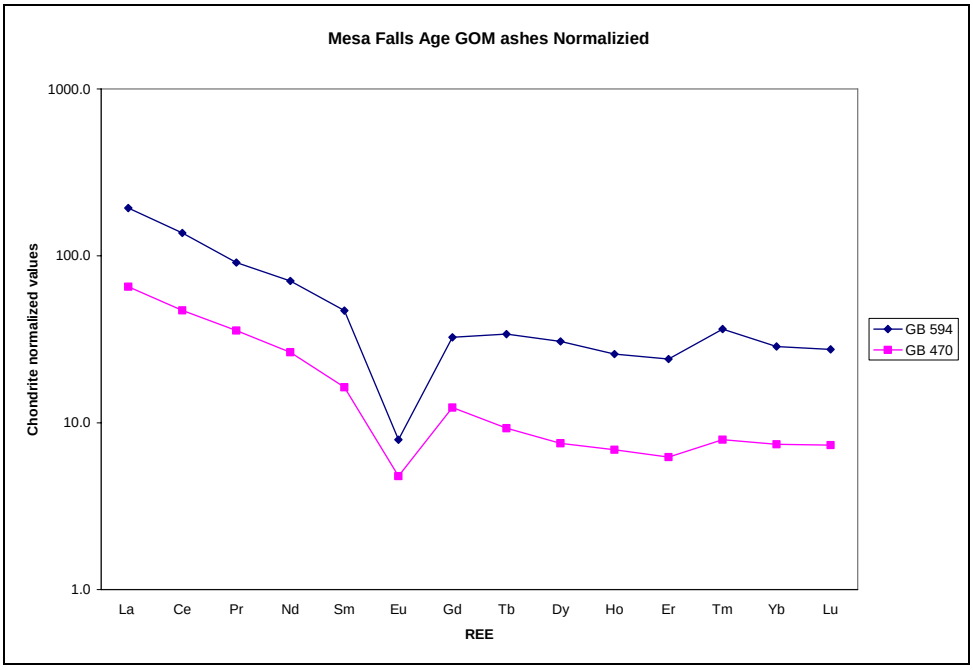

Figure 5.5 REE plot for Mesa Falls age GOM ash samples.

REE patterns for the Mesa Falls equivalent aged ash are presented in Figure 5.5. The REE values for the two samples differ considerably, with GB 470 having significantly lower REE concentrations. They are similar in LREE fractionation, but have a different Eu anomaly and HREE slope. GB 594 actually is similar to the HR-aged ash, as seen below.

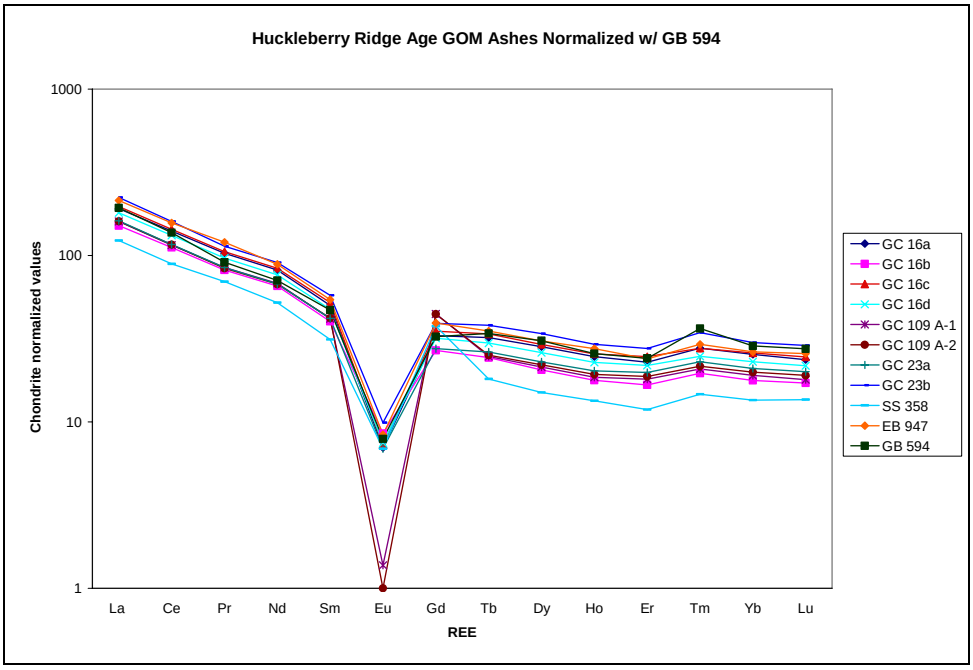

Figure 5.6 REE plot of the Huckleberry Ridge age ashes with GB 594 included (dark green line).

Shown above is the same REE Huckleberry Ridge-aged ash diagram, with the anomalous Mesa Falls GB 594 included. GB 594 is consistent with the HR-aged samples in every respect, which suggests that the sample could actually be reworked Huckleberry Ridge aged ash deposited within younger Mesa Falls-aged sediments. GB 594 had poorly constrained paleo data (1.04 – 1.15 Ma), consistent with reworked material.

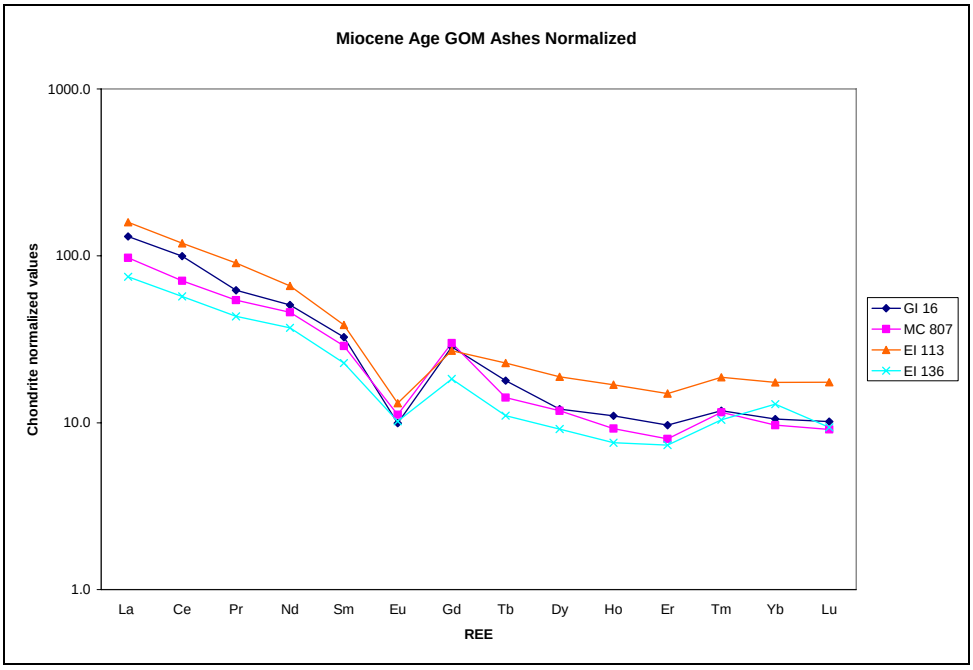

Figure 5.7 REE plot of the Miocene age GOM ashes.

Figure 5.7 shows the REE variation amongst the Miocene-aged samples. The samples show similar Eu values, with similar HREE fractionation. Variations in the REE curves show a trend of increasing fractionation (EI 136 to EI 113). The Eu anomaly is much less negative than the younger ash samples.

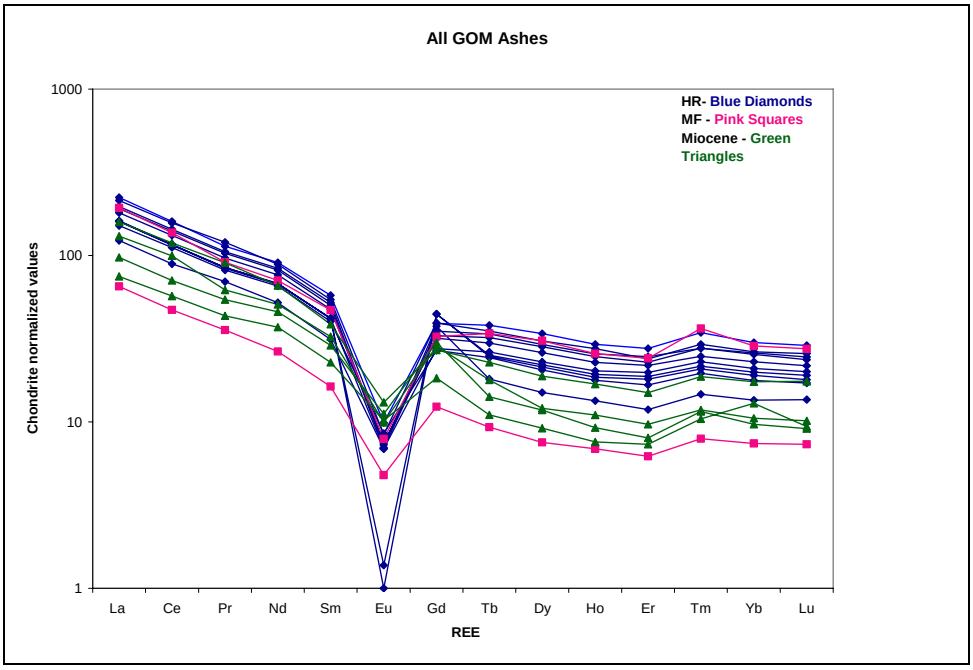

Figure 5.8 REE plot for all GOM ashes.

Figure 5.8 displays the REE pattern for all 16 GOM ash samples. The general trend towards a more negative Eu anomaly from old to young ashes is evident (Miocene in green, Huckleberry Ridge in blue, and Mesa Falls in pink). The major exception is the HR-aged ash from GC 109). The more fractionated melt should have the most negative Eu anomaly. If the GB 594 sample is excluded, based upon its similarity to HR aged samples, this is the trend seen. The oldest, Miocene aged samples have the least negative anomaly, followed by the HR-aged samples (excluding GC 109), and then the youngest Mesa Falls samples.

Trace Element Discrimination

The central question of this study remains; can the Huckleberry Ridge, Mesa Falls, and Miocene-aged ashes be differentiated with trace and REE? Variations of REE and other trace element ratios were examined to answer this question. Presented in this section are the graphical results of the variations in various trace elements.

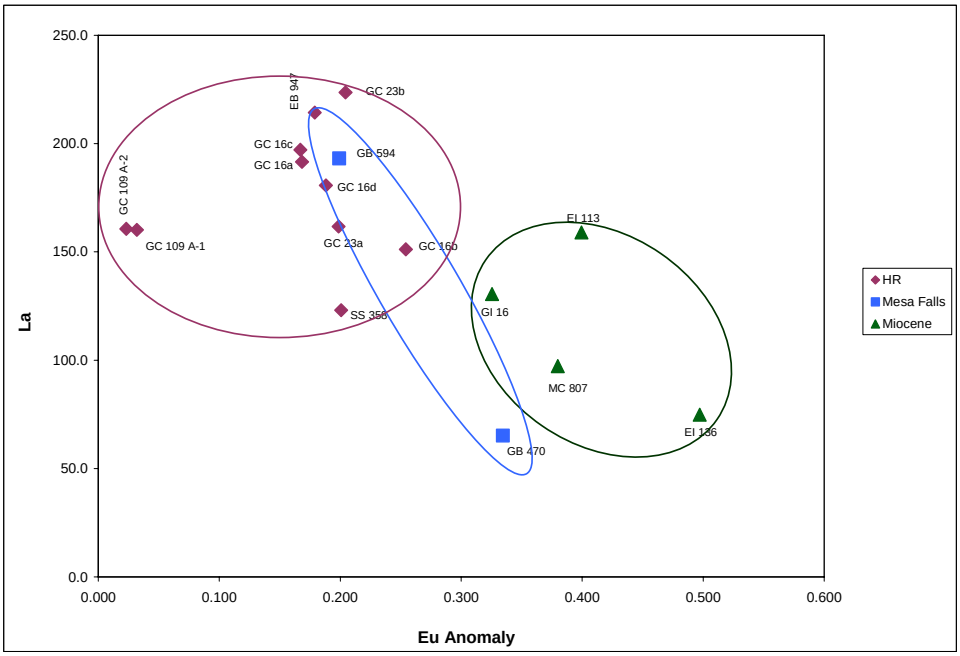

Figure 5.9 Plot of the Eu Anomaly verses La for the GOM ashes.

Figure 5.9 illustrates the range of the Eu anomaly versus La concentration. The Miocene and Huckleberry Ridge equivalent aged ashes are easily distinguished using these values. The Mesa Falls ashes are somewhat separated. Clearly a lack of samples and the probability of the GB 594 being reworked Huckleberry Ridge limits the ability to identify the Mesa Falls ash.

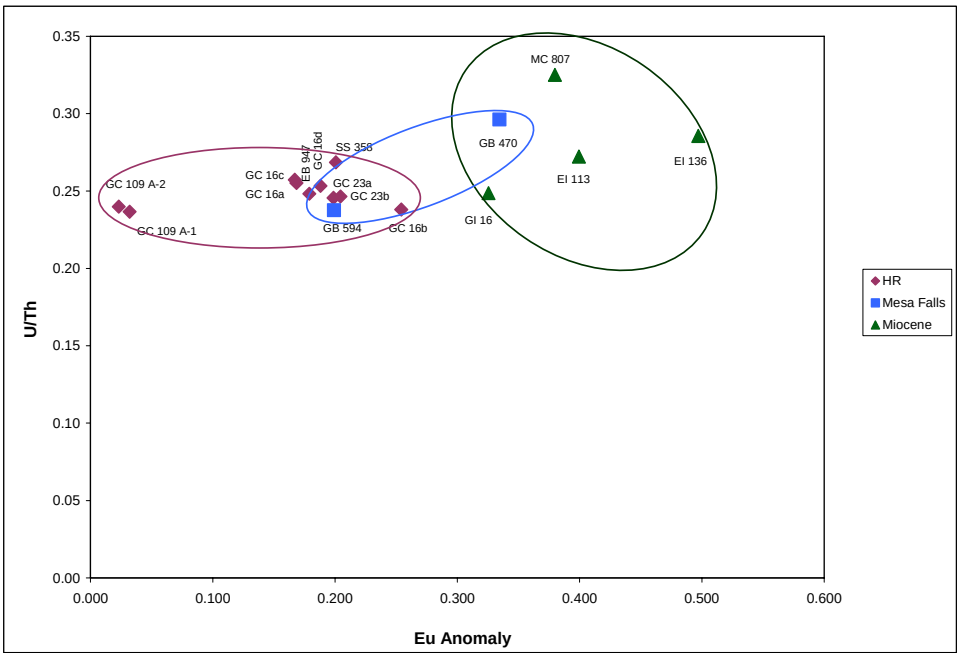

Figure 5.10 Plot of the Eu Anomaly verses the U/Th ratio for the GOM ashes.

The U/Th ratio shows a pronounced division between the three ashes with more tightly clustered groups compared to La in Figure 5.9. The Huckleberry Ridge age samples range from 0.1 to 0.3 for the Eu anomaly with two outliers, GC 109 A-2 and A-1. The Miocene age samples show some scatter but all range from 0.3 to 0.6 for the Eu anomaly with the Mesa Falls GB 470 falling within that range. GB 594 falls within the Huckleberry Ridge field, consistent with previous diagrams.

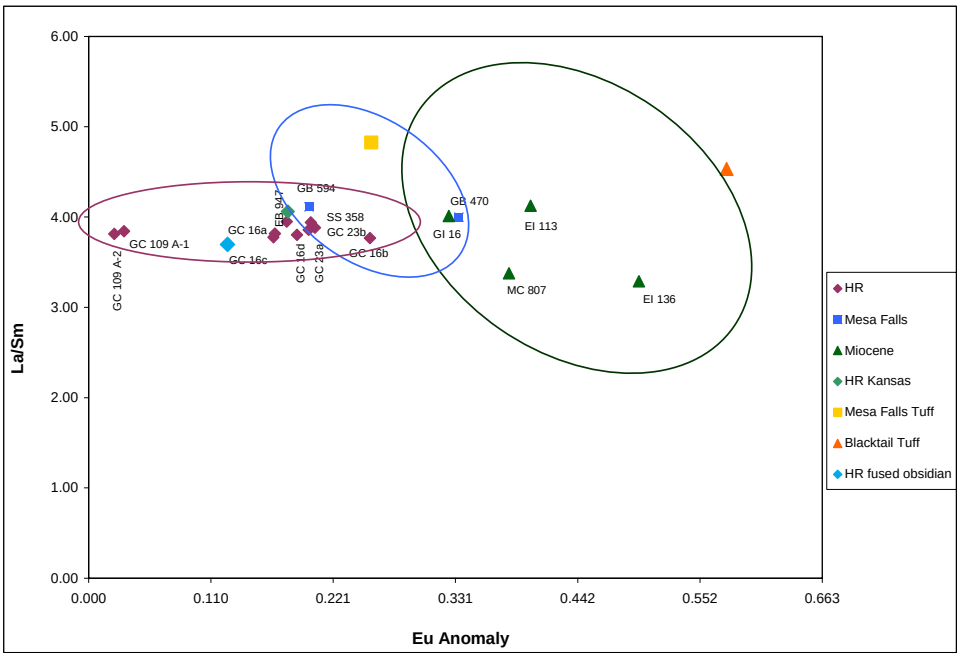

Figure 5.11 Plot of the Eu Anomaly verses the La/Sm ratio for the GOM ashes.

Figure 5.11 shows the variation between the Eu anomaly and the fractionation of the LREE for all of the samples. The Miocene ashes can be discriminated from the Huckleberry Ridge aged ash, with the Mesa Falls plotting in-between. Additional samples from previous research of known SRP/Yellowstone eruptions are plotted for comparison. The Mesa Falls Tuff and Miocene Blacktail Tuff are whole rock values from Christiansen (2001) and Morgan et al., (1984) respectively. The HR fused obsidian from Yellowstone is from Christiansen (2001). The Huckleberry Ridge sample from Kansas was prepared and analyzed using identical methods to this study, and have been independently dated as Huckleberry Ridge using fission track methods (Naeser et al., 1973). The two HR samples (Kansas and the fused obsidian) plot within the range of the HR aged ash GOM samples. The Mesa Falls Tuffs from the GOM and Yellowstone show a significant amount of scatter predominantly due to different analytical methods used to generate the LREE values. The Miocene Blacktail Tuff and Miocene GOM ashes also exhibit a large range of values due to differing analytical methods.

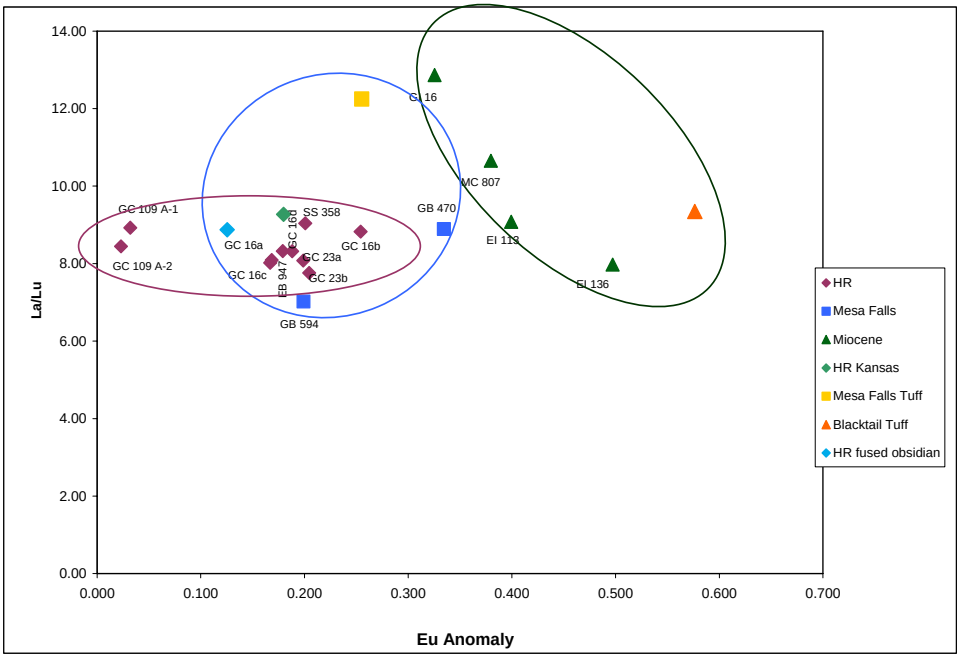

Figure 5.12 Plots of the Eu anomaly verses the La/Lu ratio for the GOM ashes.

The best discrimination between ashes is seen by comparing the Eu anomaly to the La/Lu ratio, which is a measure of light rare-earth elements to the heavy rare-earth element fractionation. The Huckleberry Ridge age samples show a very consistent La/Lu value. The values from previous research plot within the fields established by the GOM samples.

Spider Diagrams

Below are spider diagrams for the Huckleberry Ridge, Mesa Falls, and Miocene aged ashes from the GOM. These diagrams were constructed using available ICPMS trace element data, and are arranged with decreasing element mobility from left to right along the x-axis. All the data are normalized relative to MORB (Pearce, 1983).

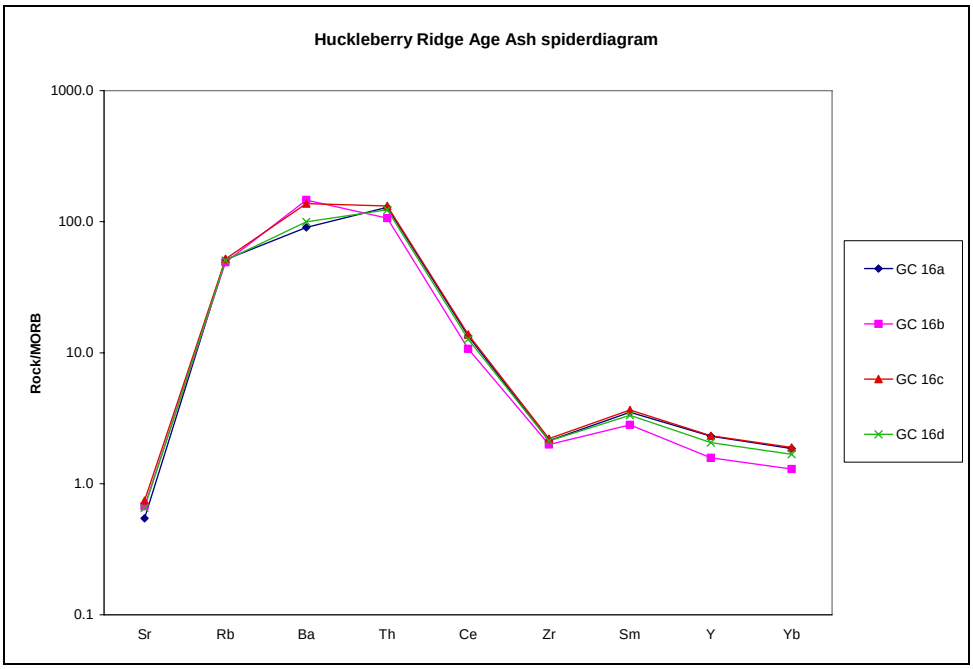

Figure 5.13 Spider plot for the GC 16 GOM ash samples.

The plot above looks at four samples from the GC 16 well collected at three separate depths. There is very little variation with the four samples associated with depth. There is a small variation in the least mobile elements (Sm, Y, Yb) between the sidewall core sample, GC 16b and the samples from well cuttings. This could be an effect of the averaging characteristics of well cuttings versus a core from a specific depth, similar to the REE variation (Figure 5.3). Ba also varies between the samples, which could be a function of diagenetic alteration.

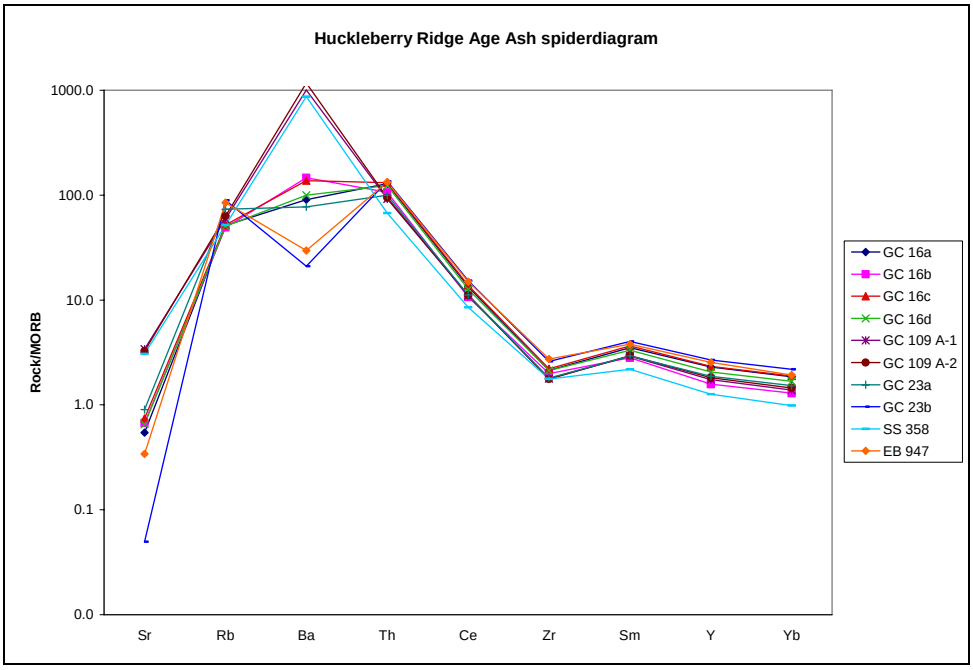

Figure 5.14 Spider plot for the Huckleberry Ridge age GOM ashes.

Figure 5.14 includes all of the HR samples from the GOM. The predominant variations are exhibited at Sr, and Ba. These elements do not vary systematically, nor does Rb, eliminating diagentic mobility as the cause for the Sr and Ba variation. The range in Ba and Sr could be from variations within original magma.

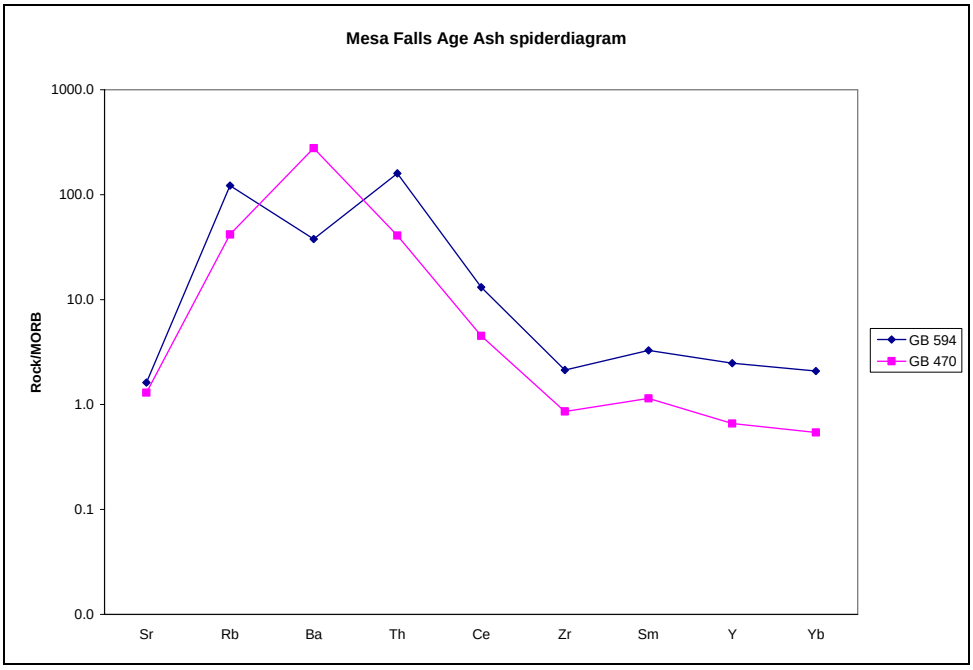

Figure 5.15 Spider plot of the Mesa Falls age GOM ashes.

GB 594 plots within a range consistent with HR trace elements seen in Figure 5.14. Little can be determined about Mesa Falls trace element behavior due to a lack of samples.

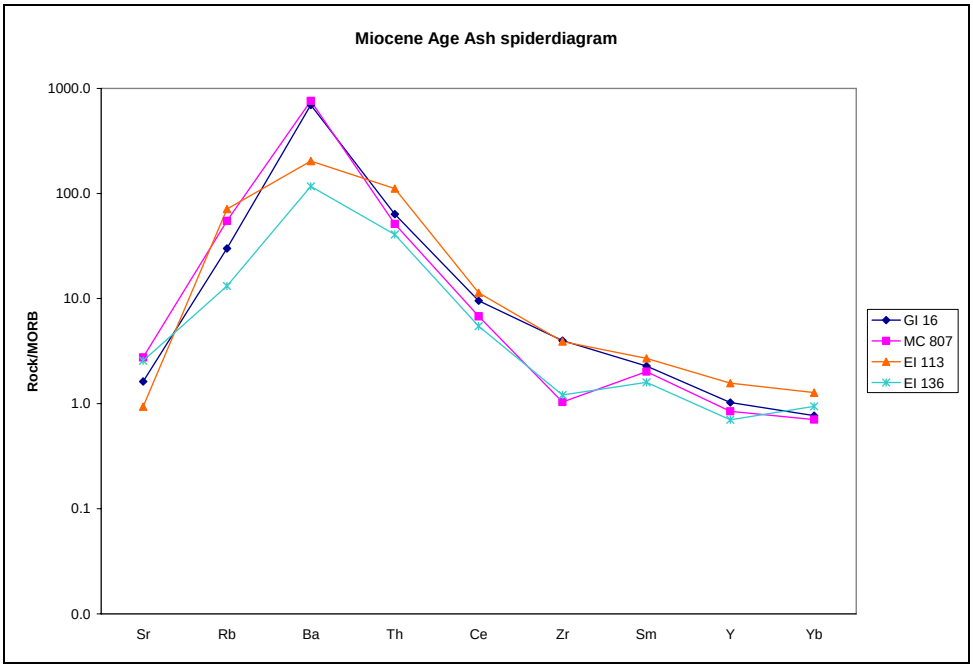

Figure 5.16 Spider plot for the Miocene age GOM ash samples.

The Miocene age samples show more variations than seen with Huckleberry Ridge age samples. The GI 16 and MC 807 show slight enrichments in Ba compared to EI 113 and EI 136. Slight scatter can be seen for Sr, Rb, Th and Ce. At Zr MC 807 and EI 136 show depletion. The variation in the trace element can be a result of either differing parental magma sources or diagenetic alteration.

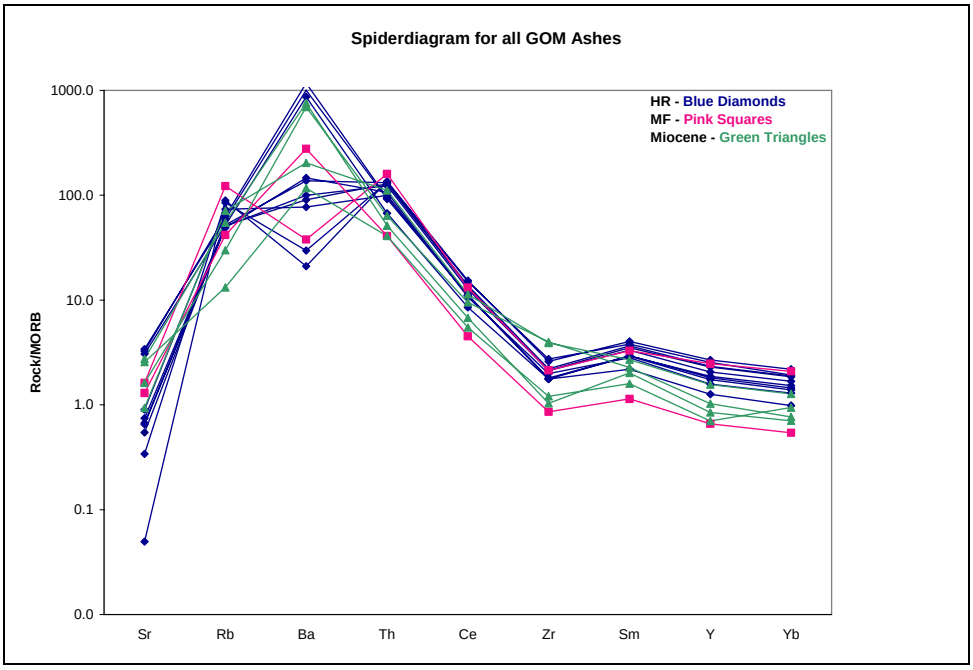

Figure 5.17 Spider plot for all GOM ashes.

The spiderdiagram above shows all 16 GOM ash samples. The Miocene age samples show Ba values in-between the enriched and depleted HR samples. Sr values for both the Miocene and Mesa Falls age samples follow the same trend as Ba. Variations within all 16 GOM samples suggest different diagenetic histories or parental magma differentiation.

Chapter 6 Conclusions

The objective for this study was to investigate the use of REE and other trace element data as a differentiation tool between GOM ashes of different ages. The paleontological ages are consistent in age with Yellowstone and the Snake River Plain (SRP). Sixteen ash samples from the GOM were analyzed geochemically with the University of Kansas ICP-MS. REE can potentially fingerprint the GOM ashes with age's

consistent with the Huckleberry Ridge, Mesa Falls, and Miocene ashes. REE distributions with depth show little variation, indicating alteration effect on the REE if any, was minimal (Figure 5.3).

The use of REE variation, such as the Eu anomaly combined with REE fractionation measures (La/Sm and La/Lu) proved to be the best fingerprinting tool (Figures 5.11 and 5.12). Two GOM Huckleberry Ridge age ashes GC 109 A-1 and A-2 show a pronounced Eu anomaly (Figure 5.4). This exaggerated anomaly could make this ash an excellent maker bed within the GOM. One anomalous Mesa Falls aged sample (GB 594) plots within the older Huckleberry Ridge ash could be a result of reworking and deposition of older ash into younger sediments. This idea is supported by both the REE plots (Figure 5.6, 5.8 and 5.9-5.12), and spiderdiagram (5.17). The data correlates with the trend of an increasing negative anomaly towards younger eruptions. The exception is the Mesa Falls sample (GB 470) (Figure 5.9 – 5.12). The Mesa Falls (1.2 Ma) sample falls between the Huckleberry Ridge (2.0 Ma) and Miocene (~ 7 Ma). This observation suggests the role of multiple magma chambers with complex fractionation histories during supervolcanic eruptions.

Direct correlation of GOM ash to Yellowstone and the Snake River Plain (SRP) is hindered by the lack of comparable REE data of glass products near the eruption. The HR aged samples from the GOM correlate very closely to ash collected from outcrops in Kansas, which are accepted as Huckleberry Ridge. In order to correlate other GOM ash beds to their eruptive sources, ash outcrops from known eruptions should be analyzed using the methods within this study.

References

Bindeman, I.N., 2006, The Secrets of Supervolcanoes: Scientific America, June, p. 36-43.

Bindeman, I.N., and Valley, J.W., 2001, Low-δ ^{18}O Rhyolites from Yellowstone: Magmatic evolution Based on Analysis of Zircons and Individual Phenocrysts: Journal of Petrology, v. 42-8, p. 1491-1517.

Christiansen, R.L., 2001, the Quaternary and Pliocene Yellowstone Plateau Volcanic Field of Wyoming, Idaho, and Montana: Geology of Yellowstone National Park Professional paper 729-G, U.S. Geological Survey, p. 1-156.

Christiansen, R.L., 1984, Yellowstone magmatic evolution: It's bearing on Understanding large-volume explosive volcanism, in Explosive volcanism; Inception, evolution, and hazards: Washington, D.C., National Academy Of Sciences, p. 84-95.

Hanna, M.A., 1926, An Interesting volcanic ash from Calcasieu Parish, Louisiana: American Association of Petroleum Geology Bulletin, v. 10, p. 93-95.

Hanan, M.A., and Totten, M.W., 1996, Analytical Techniques for the Separation and SEM Identification of Heavy Minerals in Mudrocks: Journal of Sedimentary Research, v. 66-5, p. 1027-1030.

Hanan, M.A., Totten, M.W., Hanan, B.B, and Kratochovil, T., 1998, Improved Regional ties to Global Geochronology Using Pb- Isotope Signatures of Volcanic Glass Shards from Deep Water Gulf of Mexico Ash Beds: Gulf Coast Association of Geological Societies Transactions, v. 45-3, p.95-106.

Henderson, P., 1996, the Rare Earth Elements; Introduction and Review: Journal of Rare Earth Minerals; Chemistry, Origin and Ore Deposits, v. 1996, p. 1-19.

Hunter, B.E., and Davies, D.K., 1979, Distribution of Volcanic Sediments in the Gulf Coastal Province; Significance of Petroleum Geology: Gulf Coast Association of Geological Societies Transactions, v. 29, p. 147-155.

Izett, G.A., and Wilcox, R.E., 1982, Map showing localities and inferred Distribution of the Huckleberry Ridge, Mesa Falls, and Lava Creek ash Beds (Pearlette family ash beds) of Pliocene and Pleistocene age in the Western United States and southern Canada: U.S. Geological Survey

Miscellaneous Investigations Map I-1325, scale 1:4,000,000.

Jurik, M.A., 2003, The Occurrence and Seismic Expression of Plio-Pleistocene Volcanic Ash Beds within the Ship Shoal, Ewing Banks, and Green Canyon Areas, Offshore Louisiana: unpublished Masters thesis, University of New Orleans, LA, pp. 102.

Kachler, K.L., 1999, the deposition and extent of Pliocene and Pleistocene volcanic Ash in the South Timbalier Region, offshore Louisiana: unpublished Masters thesis, University of New Orleans, LA, pp. 94.

Kennett, J.P., and Huddleston, P., 1972, Late Pleistocene Paleoclimatology, Foraminifera Biostratigraphy and Tephrochronology, Western Gulf of Mexico: Quaternary Research, New York, v. 2, no. 1, p. 38-69.

Kratochvil, T.M., 1997, Volcanic ashes offshore Louisiana in the northern Gulf of Mexico: unpublished Masters Thesis, University of New Orleans, LA.

Ledbetter, M.T., 1985, Tephrochronology of marine tephra adjacent to Central America: Geological Society of America Bulletin, v.96, p. 77-82.

Luedke, R.G., and Smith, R.L., 1991, Quaternary Volcanism In the Western Conterminous United States, in Morrison, R.D., ed., Quaternary Nonglacial Geology; Conterminous U.S.: Boulder, Colorado, Geological Society of America, The Geology of North America, v. K-2, p. 75-92.

McBride, B.C., Weimer, P., and Rowan, M.G., 1998, The Effect of Allochthonous Salt on the Petroleum Systems of Northern Green Canyon and Ewing Bank (Offshore Louisiana), Northern Gulf of Mexico: The American Association of Petroleum Geologist Bulletin, v. 82, no. 5B, p.1083-1112.

Moreno, Iris M., 1994, Petrogensis of Rhyolitic Ash Flow Tuffs, Southern Sierra Madre Occidental, Jalpa, Zacatecas, Mexico: unpublished Master thesis, University of New Orleans, LA.

Morgan, L.A., Doherty, D.J., and Leeman, W.F., 1984, Ignimbrites of the eastern Snake River Plain: Evidence for major caldera-forming eruptions: Journal of Geophysical Research, v. 89, p. 8665-8678.

Naeser, C.W., Izett, G.A., and Wilcox, R.E., 1973, Zircon fission-track ages of Pearlette Family ash beds in Meade County Kansas: Geology, v. 1, no. 4, p. 187-189.

Pearce, J.A., 1983, the Role of Sub-Continental Lithosphere in Magma Genesis at Active Continental Margins, in Hawkesworth, C.J. and Norry, M.J., eds., Continental Basalts

and Mantle xenoliths: Nantwich, United Kingdom, Shiva, p. 230-249

Perkins, M.E., Brown, F.H., Nash, W.P, McIntosh, W., and Williams, S.K., 1998, Sequence, Age, and Source of Silicic Fallout Tuffs in Middle to Late Miocene Basins of the northern Basin and Range Province: GSA Bulletin, v. 110, p. 344-360.

Perkins, M.E., and Nash, B.P., 2002, Explosive Silicic Volcanism of the Yellowstone Hotspot: The Ash Fall Tuff Record: GSA Bulletin, v. 114, p. 367-381.

Rather, M.A., 1999, the Occurrence and Diagenesis of Plio-Pleistocene Volcanic Ash within the Ewing Bank and Green Canyon Areas, Offshore Louisiana: Unpublished Masters Thesis, University of New Orleans, LA, pp.87.

Steiner, R.J., 1973, Grand Isle Block 16 Field Offshore Louisiana, in Braunstein, J., Hartman, J.A., Kane, B.L., and Van Amringe, J.H., ed., Offshore Louisiana Oil and Gas Fields: Lafayette and New Orleans Geological Society, v. October 1973, p. 65-74.

Taylor, S.R., and Mclennan, S.M., 1995, the Geochemical Evolution of the Continental Crust: Reviews of Geophysics, v. 33, p. 241-265.

Totten, M.W., Hanan, M.A., Knight, D., and Borges, J., 2002, Characteristics of Mixed-layer Smectite/Illite Density Separates during Burial Diagenesis: American Mineralogist, v. 87, p. 1571-1579.

Totten, M.W., Jurik, M.A., and Hanan, M.A., 2005, the Occurrence and Seismic Expression of Volcanic Ash Beds in the Gulf of Mexico: Gulf Coast Association of Geological Societies Transactions, v. 55, p. 810-820.

Totten, M.W., Sr., Simpson, S., Powers, E., and Totten, I.M., 2007, The occurrence and Distribution of sedimentary zeolites in the Main Pass Area, Gulf of Mexico Basin: Gulf Coast Assoc. Geological Society Transactions, v. 57, p. 717-727.

Van Fleet, J.S., Totten, M.W., and Hanan, M.A., 1999, Investigation of the Pleistocene ashes of Kansas; Identification based upon chemical Characteristics: Geological Society of America Abstracts with Programs, v. 30, p. A55.

Walton, A.W., 1986, Effect of Oligocene volcanism on sedimentation in the Trans-Pecos volcanic field of Texas: Geological Society of America Bulletin, v. 97, p. 1192-1207.

Weimer, P., Rowan, M.G., McBride, B.C., and Kligfield, R., 1998, Evaluating the Petroleum Systems in the Northern Deep Gulf of Mexico through Integrated Basin Analysis: An Overview: The American Association for Petroleum Geologists Bulletin, v. 82 no. 5B, p. 865-877

www.geo.ku.edu/programs/researchFacilities/PALwebPage0311/PALpageFacMS.htm

Gulf of Mexico leasing map, 2007, Mineral Management Services Open File Report www.gomr.mms.gov/homepg/lsesale/opd2.pdf.